JOURNAL OF PETROLOGY | VOLUME 48 | NUMBER 7 | PAGES 1387–1409 | 2007 | doi:10.1093/petrology/egm023

Fe-rich Dunite Xenoliths from South African Kimberlites: Cumulates from Karoo Flood Basalts

TATJANA REHFELDT[1]*, DORRIT E. JACOB[1], RICHARD W. CARLSON[2] AND STEPHEN F. FOLEY[1]

[1]MAINZ UNIVERSITY, DEPARTMENT OF GEOSCIENCES, BECHERWEG 21, D-55099 MAINZ, GERMANY
[2]CARNEGIE INSTITUTION OF WASHINGTON, DEPARTMENT OF TERRESTRIAL MAGNETISM, 5241 BROAD BRANCH ROAD, NW, WASHINGTON, DC 20015, USA

RECEIVED FEBRUARY 24, 2006; ACCEPTED APRIL 2, 2007
ADVANCE ACCESS PUBLICATION MAY 28, 2007

Fe-rich dunite xenoliths within the Kimberley kimberlites comprise olivine neoblasts with minor elongated, parallel-oriented ilmenite, and rarely olivine porphyroclasts and spinel. Compared with typical mantle peridotites, olivines in the Fe-rich dunites have lower forsterite (Fo_{87-89}*) and NiO contents (1300–2800 ppm), which precludes a restitic origin for the dunites. Chrome-rich spinels are remnants of a metasomatic reaction that produced ilmenite and phlogopite. Trace element compositions differ between porphyroclastic and neoblastic olivine, the latter having higher Ti, V, Cr and Ni and lower Zn, Zr and Nb contents, documenting their different origins. The dunites have high *$^{187}Os/^{188}Os$* ratios (0·11–0·15) that result in young model ages for most samples, whereas three samples show isotopic mixtures between Phanerozoic neoblasts and ancient porphyroclastic material. Most Fe-rich dunite xenoliths are interpreted to be recrystallized cumulates related to fractional crystallization of Jurassic Karoo flood basalt magmatism, whereas the porphyroclasts are interpreted to be remnants from a much earlier (probably Archaean Ventersdorp) magmatic episode. The calculated parental magma for the most primitive olivine neoblasts in the Fe-rich dunites is similar to low-Ti Karoo basalts. Modelling the crystal fractionation of the inferred parental magma with pMELTS yields element fractionation trends that mirror the element variation of primitive low-Ti Karoo basalts.*

KEY WORDS: *dunite xenoliths; fractional crystallization; Karoo; large igneous province; pMELTS; Re–Os; trace elements*

INTRODUCTION

Kimberlites of the Kaapvaal craton in southern Africa contain large quantities of mafic and ultramafic xenoliths that have been intensively studied over the last 40 years (Carswell & Dawson, 1970; Nixon & Boyd, 1973; Gurney & Harte, 1980; Boyd, 1989; Gurney *et al.*, 1991; Pearson *et al.*, 2003). Eclogite and peridotite xenoliths in particular have been targeted for investigation in order to study the lithospheric mantle of the Archaean Kaapvaal craton (e.g. MacGregor & Carter, 1970; Gurney & Harte, 1980; Erlank *et al.*, 1987; Taylor, 1993; Shirey *et al.*, 2001; Jacob *et al.*, 2003; Schmickler *et al.*, 2004; Dawson, 2004). With a few exceptions, these studies have neglected dunite xenoliths, whose depth of origin and temperature of equilibration are difficult to constrain because of their simple mineralogy.

Dunite xenoliths are found in numerous localities worldwide (e.g. Boyd & Nixon, 1975; Rudnick *et al.*, 1993; Neumann *et al.*, 1995; Kubo, 2002; Rehfeldt *et al.*, 2006). Gurney & Harte (1980) classified dunites into two subgroups, a high forsterite group (IIIa) with olivines of Fo_{93-95}, which are the most refractory xenolith type found in kimberlites, and a low forsterite group (IIIb) with olivines of Fo_{88-90}, which are interpreted as magnesian cumulates. Some group IIIa dunites have experienced a metasomatic overprint that introduced Fe, Ti, Al, Ca, K, Na and Cr (Harte *et al.* 1975; Boyd *et al.*, 1983; Rudnick *et al.*, 1993). Group IIIb dunites with low forsterite contents of Fo_{87-89} and a sheared texture have been described from northern Lesotho and the Frank Smith kimberlite near Kimberley, RSA (Boyd & Nixon, 1975) and interpreted to

---

*Corresponding author. Telphone: 0049-6131-3922370. Fax: 0049-6131-3923070. E-mail: rehfeldt@uni-mainz.de

be of cumulate origin because of their Fe-rich nature. Abundant dunite xenoliths have also been described from western Greenland (Scott, 1981; Scott Smith, 1987), and have been interpreted as metasomatically overprinted cumulates. An origin for the Fe-rich dunite xenoliths of the Kaapvaal Craton as cumulates of Karoo basalts was first suggested by Dawson *et al.* (1981).

Here, we report major and trace element, and oxygen isotope compositions of constituent minerals and Re/Os isotope systematics of olivine separates and whole-rocks from Fe-rich dunite xenoliths from Kimberley to assess a possible cumulate origin and the age of formation. Integrating these data with calculations of the compositions of the magma in equilibrium with the olivine neoblasts in the dunite xenoliths, we test the hypothesis that the origin of these dunites is linked to Karoo basalt magmatism.

SAMPLE LOCALITY

The dunite samples are part of a new collection from the Boshof Road dump, Northern Cape Province, South Africa. Sample AJE410 was provided by the University of Cape Town (RSA) and is part of the A. J. Erlank collection. The samples are by-products of diamond mining at the DuToitspan, Bultfontein and Kimberley kimberlite pipes. The Kimberley group of kimberlites is found close to the town of Kimberley, RSA, within the southern low-Ti part of the Jurassic Karoo basalt province (183 ± 1 Ma; Cox *et al.*, 1967; Duncan *et al.*, 1997) and adjacent to the Archaean Ventersdorp volcanic series (∼2·7 Ga; Crow & Condie, 1988; Fig. 1). The kimberlites were emplaced during the Cretaceous at 86 ± 3 Ma (Allsopp & Barrett, 1975; Davis, 1977). All kimberlites of the Kimberley cluster are Group I kimberlites and originate from an undifferentiated to slightly depleted mantle source (Smith, 1983; Le Roex *et al.*, 2003). These kimberlites contain xenoliths of both dunite types (Gurney & Harte, 1980): Group IIIa and Group IIIb. The former Group IIIa dunites contain highly forsteritic olivine, and are coarse-grained granular rocks similar in appearance to peridotite xenoliths. The second type, Group IIIb, contain olivine with lower forsterite contents and are fine-grained, recrystallized, granular to porphyroclastic dunites. This study concentrates on the Group IIIb dunites (Table 1).

ANALYTICAL METHODS

Major element compositions of olivine, spinel, ilmenite and phlogopite in the dunite xenoliths were analysed with a JEOL JXA 8900 RL electron microprobe at the Department of Geosciences, Johannes Gutenberg-University, Mainz, Germany, using wavelength-dispersive analysis and a range of natural and synthetic standards (Table 2). The data were corrected using the CITZAF procedure (Armstrong, 1995); detection limits were between 0·01 and 0·07 wt %. Fluorine in phlogopite had detection limits of 0·17 wt %.

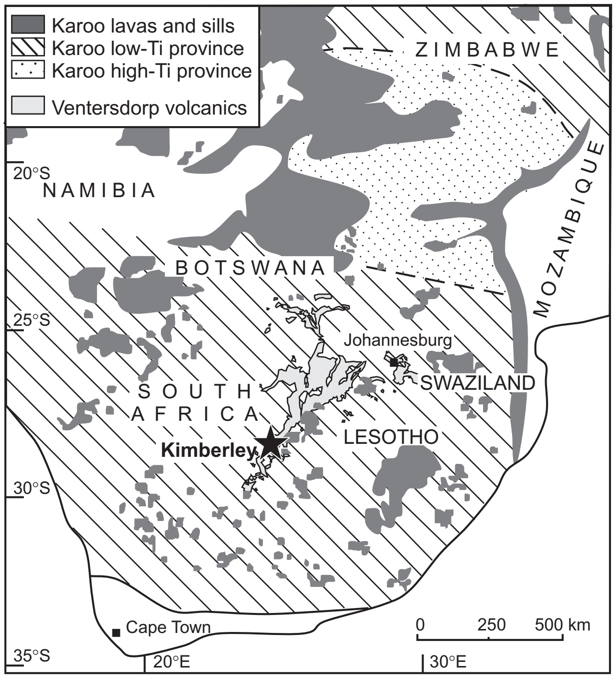

Fig. 1. Map of the Archaean Ventersdorp Supergroup and Jurassic Karoo flood basalt province in southern Africa showing Karoo low-Ti and high-Ti basalt sub-provinces (modified after Ellam & Cox, 1991; Eglington & Armstrong, 2004; Jourdan *et al.*, 2004). The Fe-rich dunite xenolith locality is Kimberley, indicated with a black star.

Table 1: Modal compositions of Fe-rich dunite xenoliths determined graphically with the ScionImage program

Sample	ol-pc	ol-nb	phl	spl	ilm	other
Fine-grained texture						
AJE410	–	98	–	1	1	–
DJ0267	–	98	1	–	1	–
DJ0268	–	99	–	–	1	–
DJ0269	–	99	–	–	1	–
Porphyroclastic texture						
DJ0270	1	98	–	–	1	–
KP0403	1	76	1	5	17	–
GB0402	55	42	2	0·5	0·5	clinopyroxene

spl, spinel; ilm, ilmenite; nb, neoblasts; ol, olivine; pc, porphyroclasts; phl, phlogopite.

Trace elements were analysed *in situ* by laser ablation–inductively coupled plasma mass spectrometry (LA-ICP-MS) in the same department using an Agilent 7500ce

Table 2: Average major and trace element compositions (and 1σ standard deviation) of the constituent minerals in Fe-rich dunite xenoliths

Sample:	AJE410						DJ0267						
Mineral:	ol		ilm		spl		ol		ilm		ilm	phl	
Comment:	neoblasts		Type II				neoblasts		Type I		Type II	metasomatic	
Major elements (wt %)													
	n = 6	1σ	*n* = 4	1σ	*n* = 3	1σ	*n* = 9	1σ	*n* = 6	1σ	*n* = 1	*n* = 4	1σ
Na_2O	<dl		0·08	±0·03	<dl		<dl		<dl		<dl	0·22	±0·05
SiO_2	39·69	±0·17	<dl		<dl		39·72	±0·27	<dl		<dl	40·62	±0·84
K_2O	<dl		<dl		<dl		<dl		<dl		<dl	10·52	±0·39
TiO_2	<dl		52·52	±0·78	7·03	±0·36	<dl		49·55	±0·43	50·20	2·66	±0·58
FeO_t	13·13	±0·18	29·68	±0·47	33·09	±0·88	12·92	±0·52	29·69	±0·29	31·03	5·09	±0·04
Al_2O_3	<dl		0·16	±0·03	5·82	±1·59	<dl		0·16	±0·04	0·12	11·38	±0·91
MgO	46·28	±0·17	12·79	±0·43	10·38	±0·43	46·83	±0·41	11·91	±0·42	12·91	23·10	±1·06
CaO	<dl		0·06	±0·02	<dl		0·05	±0·02	0·05	±0·02	0·15	<dl	
Cr_2O_3	<dl		3·80	±0·41	41·39	±0·57	<dl		6·92	±0·32	3·20	0·81	±0·54
MnO	0·13	±0·03	0·23	±0·03	0·22	±0·04	<dl		0·24	±0·03	0·29	0·04	±0·01
NiO	0·31	±0·02	0·25	±0·03	0·26	±0·04	0·29	±0·05	0·22	±0·04	0·15	0·19	±0·03
Cl	nd	nd	nd	nd	nd	nd	nd	nd	nd	nd	nd	0·02	±0·01
F	nd	nd	nd	nd	nd	nd	nd	nd	nd	nd	nd	0·77	±0·56
Total	99·54		99·57		98·19		99·92		98·74		98·05	95·42	
Mg-no.	0·87		0·42		0·45		0·88		0·42		0·43	0·89	
$\delta^{18}O$ (‰)	nd		nd		nd		5·22		nd		nd	nd	
Trace elements (ppm)													
	n = 6	1σ	*n* = 4	1σ	*n* = 2	1σ	*n* = 8	1σ	*n* = 4	1σ			
Sc	3·190	±0·520	29·8	±0·4	4·51		3·45	±0·62	35·8	±2·3			
Cr	196	±9	29600	+3700	IST		156	±18	46800	±2200			
Co	138	±1	315	±8	395	±27	135	±4	224	±19			
Ni	nd		2790	±90	3060	±10	2260	±80	1980	±220			
Cu	2·47	±0·69	61·5	±7·0	104	±11	4·81	±2·22	33·6	±9·2			
Zn	nd		472	±1	2240	±70	79·5	±5·2	253	±49			
Y	<dl		0·615	±0·099	2·55		<dl		0·301	±0·336			
Ti	125	±14	IST		35400	±200	110	±22	IST				
V	3·43	±0·21	1060	±60	1510	±100	3·25	±0·84	1180	±50			
Zr	0·284	±0·094	858	±9	15·0	±5·5	0·533	±0·216	601	±79			
Nb	<dl		552	±23	2·96	±1·64	<dl		796	±25			
Hf	<dl		25·6	±1·6	1·62		<dl		22·7	±3·2			
Ta	<dl		77·0	7·9	<dl		<dl		116	±8			
Ca	407	±78	1100	±250	<dl		nd		nd				
Li	4·03	±0·42	5·03	±1·07	<dl		3·72	±0·52	3·60	±0·85			
B	<dl		nd		nd		<dl		nd				
Rb	nd		nd		nd		nd		nd				
Sr	<dl		nd		nd		<dl		nd				
Ba	<dl		40·8		<dl		<dl		<dl				
Ga	<dl		8·05	±2·62	78·9	±2·6	<dl		7·46	±1·19			
Ge	nd		<dl		<dl		nd		<dl				
Sn	nd		5·95		5·67	±1·56	nd		7·96	±1·25			
Sb	nd		<dl		<dl		nd		<dl				
Pb	nd		1·26		<dl		nd		4·41	±1·77			
U	nd		0·164	±0·019	<dl		nd		<dl				

Abbreviations as in Table 1, plus: dl, detection limit; FeO_t, total iron as ferrous iron; IST, internal standard; Mg-number = $Mg/(Mg + Fe^{2+})$; *n*, number of measurements; nd, not determined.

(continued)

Table 2: Continued

Sample:	DJ0268				DJ0269				DJ0270			
Mineral:	ol		ilm		ol		ilm		ol		ol	
Comment:	neoblasts		Type I		neoblasts		Type I		porphyroclasts		neoblasts	
Major elements (wt %)												
	$n=6$	1σ	$n=6$	1σ	$n=6$	1σ	$n=3$	1σ	$n=2$	1σ	$n=5$	1σ
Na_2O	<dl		nd		<dl		nd		<dl		<dl	
SiO_2	40·81	±0·28	<dl		39·82	±0·14	<dl		40·04	±0·01	39·64	±0·11
K_2O	<dl		nd		<dl		nd		<dl		<dl	
TiO_2	<dl		48·86	±0·11	<dl		48·01	±0·16	nd		nd	
FeO_t	11·59	±0·12	30·32	±0·80	11·81	±0·31	30·84	±0·20	10·46	±0·12	11·98	±0·14
Al_2O_3	<dl		0·60	±0·09	0·03	±0·01	0·58	±0·09	<dl		<dl	
MgO	47·48	±0·19	11·96	±0·30	47·71	±0·34	11·73	±0·14	49·21	±0·04	47·63	±0·21
CaO	<dl		0·03	±0·01	<dl		nd		<dl		<dl	
Cr_2O_3	<dl		7·23	±0·59	<dl		6·73	±0·26	<dl		<dl	
MnO	0·14	±0·02	0·20	±0·02	0·12	±0·02	0·20	±0·01	0·14	±0·04	0·13	±0·02
NiO	0·33	±0·07	0·25	±0·03	0·32	±0·07	0·23	±0·03	0·22	±0·01	0·35	±0·04
Cl	nd		nd		nd		nd		nd		nd	
F	nd		nd		nd		nd		nd		nd	
Total	100·35		99·45		99·81		98·32		100·07		99·73	
Mg-no.	0·88		0·41		0·89		0·40		0·91		0·89	
$\delta^{18}O$ (‰)	nd		nd		nd		nd		5·14		nd	
Trace elements (ppm)												
	$n=6$	1σ	$n=5$	1σ	$n=6$	1σ	$n=3$	1σ	$n=4$	1σ	$n=6$	1σ
Sc	5·79	±0·86	26·6	±4·0	5·13	±0·09	34·2	±6·7	2·36	±0·21	2·75	±0·15
Cr	236	±4	47000	±6300	258	±5	51000	2900	66·0	±7·5	234	±16
Co	145	±2	223	±19	163	±3	212	±6	116	±8	130	±6
Ni	2340	±90	2420	±360	2790	±100	2200	±70	nd		nd	
Cu	3·17	±0·21	41·4	±8·1	3·55	±0·15	26·9	±1·1	1·10	±0·33	2·87	±0·22
Zn	78·3	±2·7	273	±63	131	±3	191	±9	67·8	±7·1	73·8	±4·3
Y	0·024	±0·007	0·171	±0·106	nd		0·294	±0·235	<dl		0·023	±0·010
Ti	304	±6	IST		296	±11	IST		151	±9	246	±23
V	5·29	±0·03	1160	±90	5·47	±0·10	1380	±110	4·43	±0·36	4·79	±0·49
Zr	0·230	±0·038	389	±56	0·224	±0·016	597	±192	0·302	±0·050	0·160	±0·031
Nb	0·024	±0·007	244	±10	0·029	±0·009	312	±55	0·101	±0·015	0·041	±0·007
Hf	<dl		12·3	±0·6	0·013	±0·002	17·8	±4·3	0·020	±0·007	<dl	
Ta	0·004	±0·013	42·0	±5·1	0·004	±0·002	52·4	±2·2	0·008	±0·001	<dl	
Ca	367	±27	nd		320	±13	<dl		192	±13	351	±35
Li	2·66	±0·07	2·85	±0·19	nd		1·68	±0·45	2·02	±0·14	2·49	±0·08
B	0·920	±0·069	nd		nd		nd		0·738	±0·171	0·556	±0·107
Rb	nd		nd		<dl		nd		nd		nd	
Sr	<dl		nd		0·007	±0·001	nd		0·045	±0·035	<dl	
Ba	<dl		<dl		<dl		0·750	±0·608	<dl		<dl	
Ga	0·154	±0·021	15·4	±2·6	nd		16·0	±1·5	0·097	±0·023	0·136	±0·020
Ge	nd		<dl		nd		2·06	±1·79	nd		nd	
Sn	nd		5·51	±3·36	nd		8·28	±1·65	nd		nd	
Sb	nd		<dl		nd		0·611	±0·433	nd		nd	
Pb	nd		3·01	±1·40	nd		75·8	±50·5	nd		nd	
U	nd		0·036	±0·028	nd		0·088	±0·069	nd		nd	

(continued)

Table 2: Continued

Sample:	DJ0270		GB0402										
Mineral:	ilm		ol		ol	ol		ilm		spl	spl	phl	
Comment:	Type I		porphyroclasts		pc rim	neoblasts		Type II					
Major elements(wt %)													
	$n=3$	1σ	$n=4$	1σ	$n=1$	$n=3$	1σ	$n=7$	1σ	$n=1$	$n=1$	$n=2$	1σ
Na_2O	nd		<dl		<dl	<dl		<dl		nd	nd	0·40	±0·002
SiO_2	<dl		40·17	±0·22	40·46	40·53	±0·16	<dl		0·07	0·08	39·45	±0·04
K_2O	nd		<dl		<dl	<dl		<dl		nd	nd	9·95	±0·01
TiO_2	47·74	±0·77	<dl		<dl	nd		52·89	±0·31	16·08	4·00	3·37	±0·08
FeO_t	30·51	±0·30	12·95	±0·84	11·77	12·61	±0·27	30·85	±0·52	47·10	29·39	5·57	±0·57
Al_2O_3	0·66	±0·08	<dl		<dl	<dl		0·12	±0·02	1·91	1·05	12·43	±0·12
MgO	11·64	±0·31	46·83	±0·60	47·54	46·98	±0·16	12·51	±0·49	9·58	8·77	23·97	±0·15
CaO	nd		<dl		<dl	0·08	±0·02	0·10	±0·02	<dl	<dl	<dl	
Cr_2O_3	7·15	±0·77	<dl		<dl	<dl		2·04	±0·40	22·63	54·81	0·54	±0·14
MnO	0·20	±0·05	0·20	±0·03	0·17	0·14	±0·01	0·32	±0·05	0·27	0·20	<dl	
NiO	0·23	±0·02	0·17	±0·08	0·28	0·30	±0·11	0·15	±0·04	0·36	0·16	nd	
Cl	nd		nd		nd	nd		nd		nd	nd	<dl	
F	nd		nd		nd	nd		nd		nd	nd	0·76	±0·07
Total	98·13		100·32		100·22	100·64		98·98		98·00	98·46	96·44	
Mg-no.	0·40		0·87		0·88	0·87		0·38		0·35	0·42	0·89	
$\delta^{18}O$ (‰)	nd		4·83*		nd	4·95		nd		nd	nd	nd	
			4·59*										
Trace elements (ppm)													
	$n=8$	1σ	$n=4$	1σ	$n=1$	$n=5$	1σ						
Sc	26·4	±2·4	5·60	±0·28	5·44	5·24	±0·19						
Cr	48200	±4200	34·7	±3·8	217	249	±20						
Co	233	±14	158	±3	173	176	±2						
Ni	nd		1280	±10	2610	2820	±140						
Cu	41·4	±1·8	<dl		nd	5·41	±5·31						
Zn	270	±54	154	±6	142	140	±6						
Y	<dl		nd		nd	nd							
Ti	IST		115	±3	269	217	±12						
V	1210	±60	2·74	±0·76	4·72	3·81	±0·27						
Zr	440	±80	0·592	±0·062	0·291	0·232	±0·036						
Nb	265	±20	0·779	±0·079	0·062	0·034	±0·017						
Hf	13·2	±2·2	0·021	±0·001	0·012	0·023	±0·014						
Ta	46·6	±4·4	0·058	±0·023	0·003	<dl							
Ca	469	±99	110	±8	392	353	±16						
Li	2·94	±0·93	nd		nd	nd							
B	nd		nd		nd	nd							
Rb	nd		<dl		<dl	<dl							
Sr	nd		<dl		0·039	0·029	±0·009						
Ba	<dl		0·198	±0·021	<dl	0·142	±0·082						
Ga	15·3	±1·8	nd		nd	nd							
Ge	<dl		nd		nd	nd							
Sn	6·19	±1·06	nd		nd	nd							
Sb	<dl		nd		nd	nd							
Pb	1·21	±0·18	nd		nd	nd							
U	<dl		nd		nd	nd							

*Oxygen isotope replicate measurements with 1σ reproducibility of ±0·12‰.

(continued)

Table 2: Continued

Sample:	KP0403									
Mineral:	ol		ol		ilm		spl		phl	
Comment:	porphyroclasts		neoblasts		Type I					
Major elements (wt %)										
	$n=2$	1σ	$n=4$	1σ	$n=8$	1σ	$n=6$	1σ	$n=6$	1σ
Na_2O	<dl		<dl		<dl		<dl		0·43	±0·03
SiO_2	40·76	±0·28	40·64	±0·06	<dl		<dl		39·53	±0·19
K_2O	<dl		<dl		<dl		<dl		9·90	±0·12
TiO_2	<dl		<dl		46·83	±0·32	6·87	±1·39	2·98	±0·15
FeO_t	11·78	±0·02	11·92	±0·27	31·14	±0·32	31·55	±2·42	4·95	±0·13
Al_2O_3	<dl		<dl		1·10	±0·08	10·81	±2·22	13·97	±0·25
MgO	47·79	±0·08	47·41	±0·48	11·02	±0·31	11·61	±0·10	23·29	±0·26
CaO	<dl		<dl		<dl		<dl		<dl	
Cr_2O_3	<dl		<dl		9·16	±0·29	38·32	±2·15	1·43	±0·10
MnO	0·16	±0·02	0·14	±0·01	0·15	±0·01	0·17	±0·03	<dl	
NiO	0·16	±0·004	0·31	±0·13	0·23	±0·02	0·27	±0·02	nd	
Cl	nd		nd		nd		nd		0·03	±0·003
F	nd		nd		nd		nd		0·44	±0·06
Total	100·65		100·42		99·63		99·60		96·95	
Mg-no.	0·88		0·88		0·39		0·49		0·89	
$\delta^{18}O$ (‰)	nd		nd		nd		nd		nd	
Trace elements (ppm)										
	$n=3$	1σ	$n=3$	1σ	$n=7$	1σ	$n=6$	1σ	$n=5$	1σ
Sc	5·00	±0·23	5·58	±0·05	30·2	±1·2	<dl		3·28	±0·29
Cr	34·6	±2·5	285	±26	65600	±2400	IST		nd	
Co	130	±6	175	±6	211	±6	338	±56	nd	
Ni	1270	±70	2850	±50	nd		nd		1290	±150
Cu	nd		3·72	±0·35	29·3	±2·6	63·0	±3·6	nd	
Zn	98·5	±4·6	112	±8	149	±14	1780	±300	nd	
Y	nd		nd		0·097	±0·008	<dl		<dl	
La	nd		nd		nd		nd		0·198	±0·088
Ce	nd		nd		nd		nd		0·404	±0·261
Nd	nd		nd		nd		nd		0·678	±0·306
Ti	98·3	±4·5	180	±64	IST		34500	±7200	nd	
V	3·03	±0·06	6·20	±2·58	1560	±40	1420	±110	128	±5
Zr	0·550	±0·023	0·532	±0·309	515	±24	8·81	±4·57	7·18	±1·11
Nb	0·333	±0·055	0·148	±0·066	430	±21	1·53	±0·69	11·1	±2·8
Hf	0·018	±0·008	<dl		18·3	±0·5	<dl		0·607	±0·231
Ta	0·029	±0·009	0·025	±0·012	72·6	±8·8	1·18	±0·21	1·66	±0·94
Ca	192	±50	395	±74	<dl		<dl		279	±47
Li	nd		nd		1·83	±0·14	2·60	±1·63	2·04	±0·78
B	nd		nd		nd		nd		nd	
Rb	<dl		<dl		nd		nd		576	±66
Sr	<dl		0·218	±0·060	nd		nd		26·0	±3·2
Ba	<dl		<dl		<dl		<dl		476	±42
Ga	nd		nd		19·8	±1·0	115	±6	nd	
Ge	nd		nd		0·817	±0·246	<dl		nd	
Sn	nd		nd		6·72	±0·55	<dl		nd	
Sb	nd		nd		0·120	±0·039	<dl		nd	
Pb	nd		nd		14·2	±3·3	21·5	±5·6	6·54	±2·07
U	nd		nd		0·039	±0·008	<dl		<dl	

Table 3: Average LA-ICP-MS detection limits (ppm) in olivine, ilmenite, spinel, phlogopite and clinopyroxene and trace element composition of BCR-2G measured as unknown, ±1σ standard deviation of n measurements

	Detection limits				BCR-2G				
	olivine	ilmenite	spinel	phlogopite	this study	1σ	*n*	literature	
Sc	0·523	1·49	4·68	1·51	34·1	±2·8	57	32·2	1
Cr	2·91	7·57	nd	nd	20·4	±10·1	57	17	2
Co	0·115	0·610	3·81	nd	38·6	±3·6	43	35·8	1
Ni	0·547	1·78	5·97	1·72	13·3	±2·0	57	11·23	1
Cu	1·05	3·34	11·2	nd	19·2	±2·8	43	18·74	3
Zn	1·53	3·97	11·7	nd	167	±25	43	163	2
Y	0·061	0·262	0·365	0·122	30·4	±2·8	49	34·3	1
La	nd	nd	nd	0·103	24·3	±1·3	14	25·2	1
Ce	nd	nd	nd	0·138	50·7	±2·1	30	53·0	1
Nd	nd	nd	nd	0·378	27·7	±1·3	14	29·8	1
Ti	2·48	nd	16·0	nd	14300	±1700	57	14090	1
V	0·184	0·756	1·56	0·542	436	±31	49	419	1
Zr	0·101	0·488	0·718	0·295	164	±16	57	190	1
Nb	0·062	0·290	0·768	0·160	12·2	±1·0	57	13·32	1
Hf	0·080	0·368	0·628	0·208	4·41	±0·49	57	5·06	1
Ta	0·033	0·153	0·256	0·105	0·758	±0·137	57	0·82	1
Ca	100	244	660	267	51200	±3500	57	48600	3
Li	0·197	0·652	2·08	0·453	10·4	±1·0	41	9·67	1
B	3·35	nd	nd	nd					
Rb	0·025	nd	nd	0·400	45·2	±4·1	22	49·6	1
Sr	0·076	nd	nd	0·199	321	±18	30	346	1
Ba	0·311	1·14	nd	1·91	660	±44	57	684	1
Ga	0·157	0·587	1·55	nd	39·2	±4·9	39	22·2	1
Ge	nd	3·81	13·7	nd	2·26	±0·21	27	1·49	4
Sn	nd	1·34	4·55	nd	2·29	±0·25	27	4·3	2
Sb	nd	0·681	2·03	nd	0·446	±0·122	27	0·303	4
Pb	nd	0·433	nd	0·420	11·6	±1·4	41	11·3	1
U	nd	0·189	0·762	0·112	1·86	±0·20	41	1·93	1

Literature data: 1, Neumann *et al.* (2002); 2, Barth *et al.* (2001); 3, Halter *et al.* (2002); 4, Zack *et al.* (2002).

quadrupole ICP-MS system coupled to a New Wave Research UP-213 laser ablation system. Measurements were carried out with laser energy densities of $\sim$6·5 J/cm^2 and helium was used as carrier gas. All measurements were performed on polished thin sections of 100 μm thickness. In olivine, spot sizes were mostly 100 μm in diameter, whereas spots as small as 30 μm were used for the smaller ilmenite grains. Electron microprobe measurements of Si for silicate minerals, Ti for ilmenite and Cr for spinel were used as internal standards to calculate concentrations from LA-ICP-MS data; external standards were NIST SRM 612 glass for silicate minerals and NIST SRM 610 glass for oxide minerals (Pearce *et al.*, 1997). US Geological Survey (USGS) reference glass BCR-2G was measured as an unknown after every seventh sample spot and is in agreement with literature data (Table 3). Data reduction was carried out using GLITTER version 4. Average detection limits in olivine, ilmenite and spinel are summarized in Table 3. Detection limits were generally higher in ilmenite and spinel than in olivine.

Optically clean mineral separates of olivine neoblasts and porphyroclasts were prepared for oxygen isotope measurements by handpicking under a binocular microscope. The grains were rinsed in water and ethanol, and analysed by laser-assisted fluorination mass spectrometry at the Department of Geology, Royal Holloway University of

London following the method of Mattey & Macpherson (1993) and Mattey (1997). All values are reported as $\delta^{18}O$ relative to Vienna–Standard Mean Ocean Water (Table 2). San Carlos Olivine (SC OL) and Gore Mountain Garnet (GMG II) were measured as standards and were reproducible within $\pm 0{\cdot}08‰$ (1σ, $n = 21$). Replicate measurements on one sample of this study yielded an external precision of 0·12‰.

Whole-rock powders for Re/Os isotope analyses were prepared with a corundum ring mill from representative sample fractions that were free of vein and rim material. Olivine separates were prepared from two samples (GB0402 and AJE410) and analysed for Re–Os isotopes for comparison with whole-rock powder analyses. Olivine separates were obtained by a four-step procedure including magnetic separation, heavy liquid separation from the 300–500 µm grain fraction using methylene iodide (3·3 g/cm^3), and hand-picking to remove remaining oxide grains under a binocular microscope, followed by rinsing with water and ethanol. The olivine separates were a mixture of neoblasts and porphyroclasts, because after crushing the porphyroclasts broke into smaller pieces and could not be distinguished optically from smaller neoblasts.

Re and Os analyses were carried out at the Department of Terrestrial Magnetism, Carnegie Institution, Washington, USA. The analyses were performed on 2 g of whole-rock powder or 1 g of olivine separate, following the procedure of Carlson *et al.* (1999). The whole-rock powder was dissolved in 3 ml concentrated HCl and 6 ml concentrated HNO_3. These large quantities of acids are necessary to avoid sample loss in the Carius tube as a result of the high viscosity of the Si-gel produced by olivine dissolution. Dissolutions of whole-rock powders contained no visible grains, whereas dissolutions of olivine separates produced residual grains that were intensely altered by the dissolution procedure. Because both sulphide and chromite are soluble in the acids used, it is likely that these residual grains were spinel or ilmenite formerly included in the olivines. After extracting Re by column chemistry and Os by extraction with CCl_4 followed by microdistillation (Carlson *et al.*, 1999), the samples were analysed by negative thermal ionization mass spectrometry using a 15 inch single-collector mass spectrometer for Re and a Finnigan Triton multicollector mass spectrometer for Os. Laboratory blanks of 2 pg Os and 1 pg Re were obtained during the course of the project.

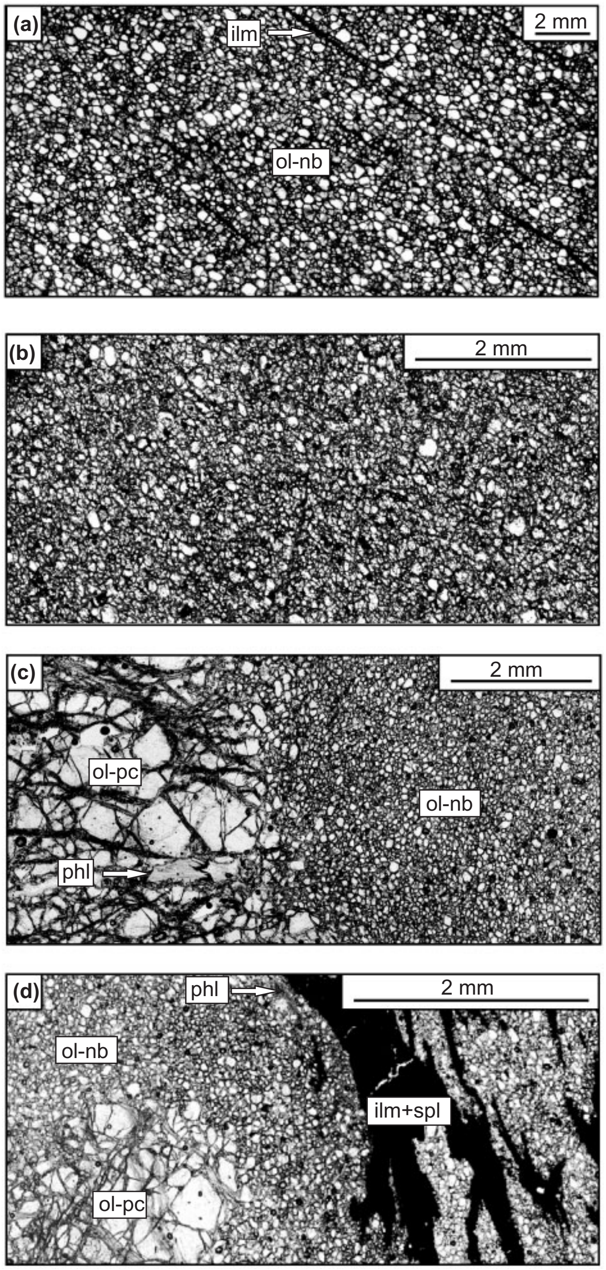

Fig. 2. Photomicrographs of representative Fe-rich dunite xenoliths: (a) granular, fine-grained olivine with parallel-oriented ilmenite (DJ0269); (b) granular, fine-grained olivine (AJE410); (c) heterogranular dunite with fine-grained olivine neoblasts and coarse olivine porphyroclasts (GB0402); (d) porphyroclastic dunite with fine-grained olivine neoblasts, coarse olivine porphyroclasts, as well as ilmenite and spinel schlieren (KP0403). Abbreviations as in Table 1.

RESULTS

Petrography and mineral chemistry

Most xenoliths studied here are fine-grained foliated rocks (samples AJE410, DJ0267, DJ0268, DJ0269; Fig. 2a and b): three samples (DJ0270, KP0403, GB0402; Fig. 2c and d) contain porphyroclasts but only sample (GB0402) is porphyroclast-rich (55%; Table 1). The fine-grained samples comprise olivine neoblasts (30–720 µm), with minor amounts of acicular ilmenites (5–280 µm) oriented parallel to the foliation, in some samples intergrown with spinel (Fig. 3). Phlogopite occurs in three samples as small, single crystals (750–140 µm) within the neoblast groundmass, in

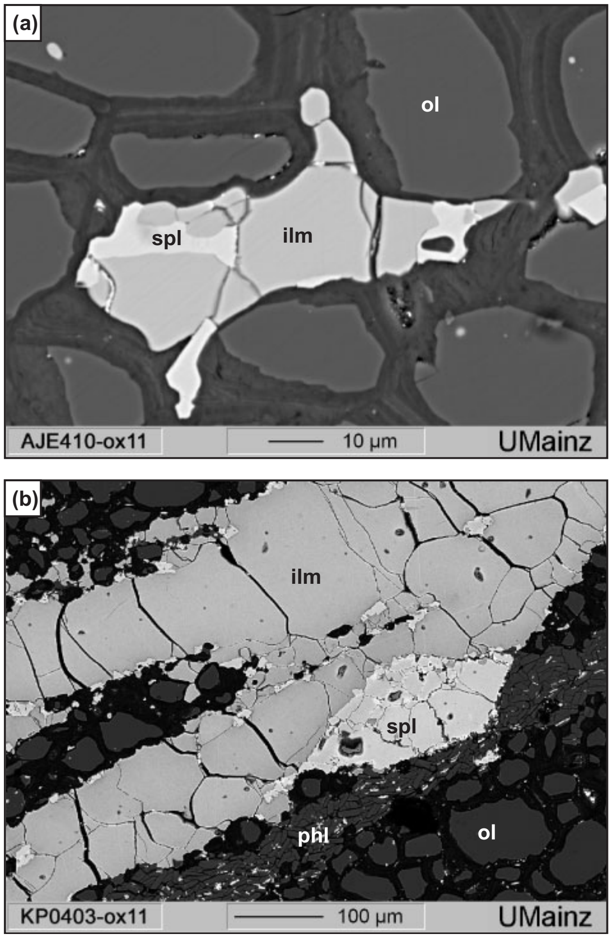

Fig. 3. Back-scattered electron images of oxide phases in Fe-rich dunite xenoliths: (a) ilmenite intergrown with chromian spinel (AJE410); (b) chromian spinel (light grey) surrounded by ilmenite (darker grey), that is formed in association with fine-grained phlogopite (KP0403). Abbreviations as in Table 1.

cracks within porphyroclasts (Fig. 2b) or together with ilmenite overgrowing spinel (Figs 2d and 3b). These textural features indicate that spinel is a pre-metasomatic phase, so that the original mineralogy was a spinel-bearing dunite. The olivine porphyroclasts are 3·5–1·1 mm in size with irregular margins that merge into the fine-grained olivine neoblast groundmass (Fig. 2c and d) and are oriented parallel to the foliation. Porphyroclasts are intensely cracked and turbid as a result of minute inclusions of oxide minerals and glass.

Porphyroclasts and neoblasts have comparable major element compositions, with forsterite contents ranging from 87 to 91. NiO contents are low (0·2–0·3 wt %) compared with olivines in typical mantle peridotites, with porphyroclastic dunites having olivine with more variable and lower NiO contents than olivine in fine-grained dunites. As a result, olivines plot away from the mantle olivine array (MOA) defined by Takahashi (1986; Fig. 4).

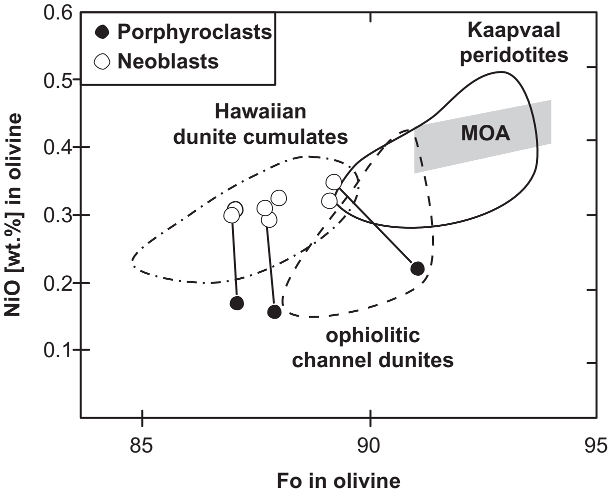

Fig. 4. NiO (wt %) vs forsterite content in Fe-rich dunite olivines compared with olivine in mantle peridotites, ophiolitic channel dunites and Hawaiian dunite cumulates (Kaapvaal peridotite: Carswell *et al.*, 1979; Simon, 2004; ophiolitic channel dunite: Suhr, 1999; Koga *et al.*, 2001; Hawaii: Clague, 1988); grey shaded field (MOA) indicates mantle olivine array of continental peridotites after Takahashi (1986).

Both fine-grained and porphyroclastic samples contain elongated ilmenite (average 20 µm width and 3 mm to 1·5 cm length) within the olivine neoblast groundmass. They often surround olivine and show reaction boundaries with it. Ilmenites have an anhedral, amoeboid appearance and are oriented parallel to the foliation (Fig. 2a and d). KP0403 is unique in having a very high modal ilmenite content (17 vol. %), which is accompanied by layers of fine-grained phlogopite oriented parallel to the ilmenite grains. In all samples, ilmenite can be divided into two types on the basis of chemical composition (Fig. 5). Both have similar MgO contents (10·5–12·9 wt %), higher than is typical for mantle-derived ilmenite (4·5–8·7 wt %; Hills & Haggerty, 1989; Zack & Brumm, 1998). Type I ilmenites have higher Al_2O_3 (0·5–1·2 vs 0·1–0·3 wt %) and Cr_2O_3 (6·3–9·5 vs 1·7–7·2 wt %), and lower TiO_2 contents (46·5–49·0 vs 49·2–53·4 wt %) than Type II ilmenites. Type II ilmenites plot in the field defined by ilmenites from Group I kimberlites (Wyatt *et al.*, 2004), supporting a secondary origin by kimberlite infiltration into the xenoliths. Both ilmenite types are distinct from ilmenites in Karoo basalts (Fig. 5), which have lower Cr_2O_3 and MgO contents. Textural evidence suggests that Type I ilmenite grew at the expense of spinel (Fig. 3), explaining the elevated Al_2O_3 and Cr_2O_3.

Spinels are remnant primary phases commonly showing reaction coronas of ilmenite and occasionally also phlogopite. They also occur as inclusions in ilmenite. Chemically, they have low Mg-number $[Mg/(Mg + Fe^{2+})]$ of 0·36–0·50, high Cr-number $[Cr/(Cr + Al)]$ of 0·67–0·97

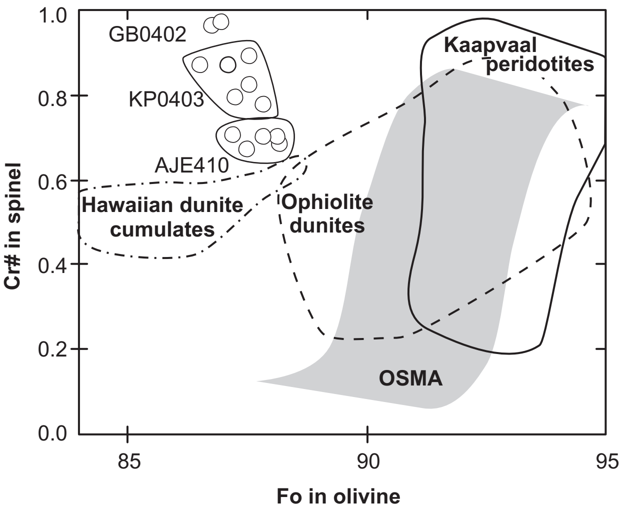

Fig. 5. Spinel Cr-number vs forsterite content of coexisting olivine in Fe-rich dunite xenoliths with compositional fields of mantle peridotites, ophiolitic and Hawaiian dunites as in Fig. 4. OSMA is olivine–spinel mantle array of Arai (1994).

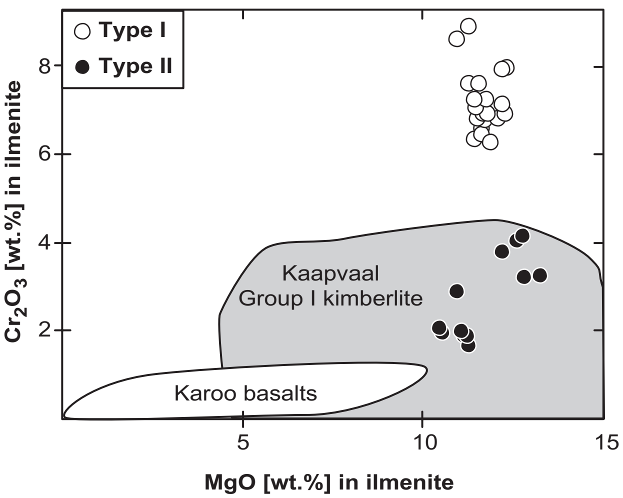

Fig. 6. Cr_2O_3 vs MgO (wt %) in ilmenites of Fe-rich dunite xenoliths, compared with ilmenite composition in Karoo basalts and group I kimberlites (Wyatt *et al.*, 2004).

and high TiO_2 contents (4–16 wt %), compared with spinel in mantle spinel peridotites of the Kaapvaal craton (Mg-number 0·48–0·78, Cr-number 0·27–0·88, $TiO_2 < 3$ wt %; Carswell *et al.*, 1979; Fig. 6). Their compositions overlap with the high-Cr-number end of the Kaapvaal peridotite array, whereas olivines lie conspicuously to lower Fo, showing no overlap (Fig. 5). However, the reaction rims around spinels indicate that spinel compositions may not reflect their original chemistry. Ilmenite and phlogopite crystallize at the expense of spinel during metasomatism, but not all the Cr from the spinel can be incorporated into ilmenite or phlogopite, so that the remaining spinel is enriched in Cr. The Type I ilmenites are very rich in Cr_2O_3 (6·3–9·5 wt %) with high Cr-number, so that the Cr-number of spinels may have increased during the metasomatic reaction, but probably only by a few per cent Cr-number (maximum 8–10%). There is no systematic compositional difference between spinels from fine-grained or porphyroclastic dunite xenoliths.

Phlogopite occurring with ilmenite in the Fe-rich dunite xenoliths has slightly lower Mg-number (0·88–0·90) and higher TiO_2 contents (1·8–3·4 wt %) compared with phlogopite in mantle peridotites (Mg-number 0·90–0·95 and TiO_2 0·1–1·9 wt %; Erlank *et al.*, 1987).

All dunites are slightly serpentinized along grain margins and in cracks within olivine porphyroclasts. Serpentine occurs with small magnetite and sulphide minerals. Only the porphyroclastic sample GB0402 contains clinopyroxene ($\ll$1%) and secondary phases such as apatite, perovskite and calcite, which are probably introduced by the kimberlite host, as they occur together with serpentine along olivine grain margins. Overall, the mineralogy of the Fe-rich dunite xenoliths is typical for dunite xenoliths from the Kaapvaal Craton (e.g. Boyd & Nixon, 1975) that are often described to contain ilmenite and other metasomatic minerals. In contrast to the dunites of the Tanzania Craton (Lee & Rudnick, 1999), the Fe-rich dunite xenoliths of this study are generally poor in chromian spinel, and chrome diopside has not been found in any thin sections.

Oxygen isotope compositions

Oxygen isotope ratios were analyzed to check the possibility that the dunite xenoliths could originate as ultramafic cumulates in the lower reaches of ocean crust or oceanic plateaux (Foley *et al.*, 2003*a*, 2003*b*). This would mean that the dunites and pyroxenites would be related to the eclogite suite xenoliths, which commonly show oxygen isotope values differing from mantle values (Jacob, 2004). It has recently been shown that fluids can circulate through cracks to very deep levels in the oceanic lithosphere and that oxygen isotopes may be influenced at much deeper levels than expected (Hart *et al.*, 1999). Olivines from the dunite xenoliths exhibit a small range of $\delta^{18}O$ values (5·14–5·22‰; Table 2) that overlaps with the $\delta^{18}O$ range of mantle peridotite olivine (5·18 ± 0·14‰; Mattey *et al.*, 1994). These data provide no evidence for exchange with seawater, but do not discount an origin as mantle samples or as cumulates from mantle-derived melts, either continental or oceanic. Sample GB0402 has a slightly lower $\delta^{18}O$ value than the average for peridotitic olivine (4·83) and duplication yielded a higher value outside the analytical uncertainty (Table 2). This is most probably the effect of minute chromite inclusions that are visible in the olivine porphyroclasts. Chromite has lower oxygen isotope values than olivine (average spinel $\delta^{18}O$ <2·5‰; Lowry *et al.*, 2003) decreasing the $\delta^{18}O$ value of the olivine.

Trace elements

Although they have Mg-number different from those of mantle peridotites, olivines in the dunite xenoliths exhibit similar trace element compositions (Fig. 7). The compositional range within the dunite xenoliths fully overlaps for V, Nb, Zr and Cr, whereas Ti contents extend to higher values than found in olivines from mantle peridotites. Ni contents in olivine porphyroclasts are lower than in mantle peridotites, whereas those of the neoblasts overlap with the peridotite field. Some trace element compositions differ between porphyroclasts and neoblasts: neoblasts are enriched in Sr, Co, Ni and Ti as well as in Ca, but depleted in Mn, Zr, Ta and Nb compared with porphyroclasts (Table 2; Fig. 7). Olivine porphyroclasts in sample GB0402 have rims that are closer in composition to neoblast compositions than the cores (Fig. 7). Olivine neoblasts have Cr and Ni contents within the compositional range of olivine in large igneous province basalts (Fe-rich dunite olivine neoblasts Cr 290–160 ppm and Ni 2850–2070 ppm compared with, for example, Etendeka olivine Cr 1200–70 ppm and Ni 4870–630; Gibson *et al.*, 2000; Thompson *et al.*, 2001), whereas porphyroclasts plot to lower values (Cr 66–35 ppm and Ni 1300 ppm; Fig. 7e).

Trace element patterns of ilmenites are compared with those of ilmenite megacrysts from kimberlites (grey field) and mantle-derived ilmenites (black field) in Fig. 8a. Ilmenite incorporates predominantly high field strength elements (HFSE) and Sc (Zack & Brumm, 1998). Compared with mantle-derived ilmenites, both types of ilmenite in the dunite xenoliths are strongly enriched in Cr. Type I ilmenites are more enriched in Cr and Ga, consistent with their growth at the expense of chromian spinel. Additionally, they are enriched in Sc and V, but depleted in Y, Cu and Zn. Both Type I and II ilmenites are characterized by higher Ni at comparable Cr than megacrystic ilmenites that are interpreted to be the cumulates of kimberlitic melts (e.g. Nowell *et al.*, 2004). Spinels (Fig. 8b) have lower HFSE and higher Zn, Cr and Ga contents than ilmenite. Their HFSE concentrations are higher than those in spinels in abyssal peridotite xenoliths (Grégoire *et al.*, 2000, 2001; Moine *et al.*, 2001), whereas the Cr contents are similar. The former may indicate overprinting by the HFSE-enriched melt or fluid from which the ilmenite crystallized.

Phlogopites have trace element compositions typical of metasomatic phlogopite in mantle peridotites (Grégoire *et al.*, 2002; van Achterbergh, 2004) with high Ba, Rb, Nb, Ta and Ti and low Ni, V, Zr, Hf, Sr, Pb and Th contents (Table 2).

Re–Os isotope systematics

The Os concentrations and isotope compositions of most dunite xenoliths are readily distinguished from those of mantle peridotites (Fig. 9). Whole-rocks have similar Re contents to Kaapvaal mantle peridotites (mostly <0·4 ppb, Fig. 9; Table 4), but on average lower Os contents (mostly <1 ppb in Fe-rich dunites, ~4 ppb in mantle peridotites). The one exception is sample GB0402, which has the high Os concentration typical of cratonic peridotites. South African kimberlites have a wider range in Re content (0·02–0·7 ppb with a mean 0·3 ± 0·2 ppb; Pearson *et al.*, 1995*a*) than the Fe-rich dunites and a similar range in Os content (0·7–3·1 ppb with a mean 1·3 ± 0·8 ppb). The $^{187}Os/^{188}Os$ ratios of most Fe-rich dunites calculated back to the age of kimberlite eruption at 86 Ma (Table 4) have a wide range and are more radiogenic than Kaapvaal mantle peridotites (γOs from −12 to 14 in dunite xenoliths vs −18 to 3 with most below −12 in mantle peridotites; Fig. 9e; Walker *et al.*, 1989; Pearson *et al.*, 1995*b*; Carlson *et al.*, 1999; Menzies *et al.*, 1999; Irvine *et al.*, 2001; Meisel *et al.*, 2001; Carlson & Moore, 2004; Simon, 2004). Again, sample GB0402 is exceptional, showing the lowest $^{187}Os/^{188}Os$ of the dunites. In contrast, kimberlite has γOs of −10 to 7 (Pearson *et al.*, 1995*a*), which is higher than Kaapvaal mantle peridotites, but not as high as the most extreme values for Fe-rich dunites. The olivine separate analyzed from GB0402 is distinguished from the whole-rock by lower Re, but higher Os concentrations (30%) with a slightly lower $^{187}Os/^{188}Os$ ratio (0·1134 vs 0·1144, respectively). In contrast, the olivine from sample AJE410 has dramatically lower Re and Os concentrations and $^{187}Os/^{188}Os$ ratio compared with the whole-rock. The tie-line connecting the Re/Os and Os isotope ratios of the olivine and whole-rock analysis from AJE410 (not shown) corresponds to an apparent 'age' in excess of 8 Ga. This must reflect the presence of an extraneous component introduced into the whole-rock that did not reach chemical and isotopic equilibrium with the constituent minerals. Along with AJE410, the ilmenite-rich sample KP0403 is the only other dunite to have an age-corrected $^{187}Os/^{188}Os$ ratio higher than the model primitive mantle. Overall, the samples show little or no correlation between Re/Os and Os isotope composition.

DISCUSSION

Metasomatic overprint

A fundamental problem frequently discussed for mantle peridotites from the Kaapvaal craton is the degree of metasomatic overprinting (Konzett *et al.*, 2000; Grégoire *et al.*, 2003). Kimberley is a particularly well-studied locality for mantle metasomatism (Erlank *et al.*, 1987; Simon *et al.*, 2007): mantle peridotite xenoliths retrieved from kimberlites of the Kimberley cluster are strongly

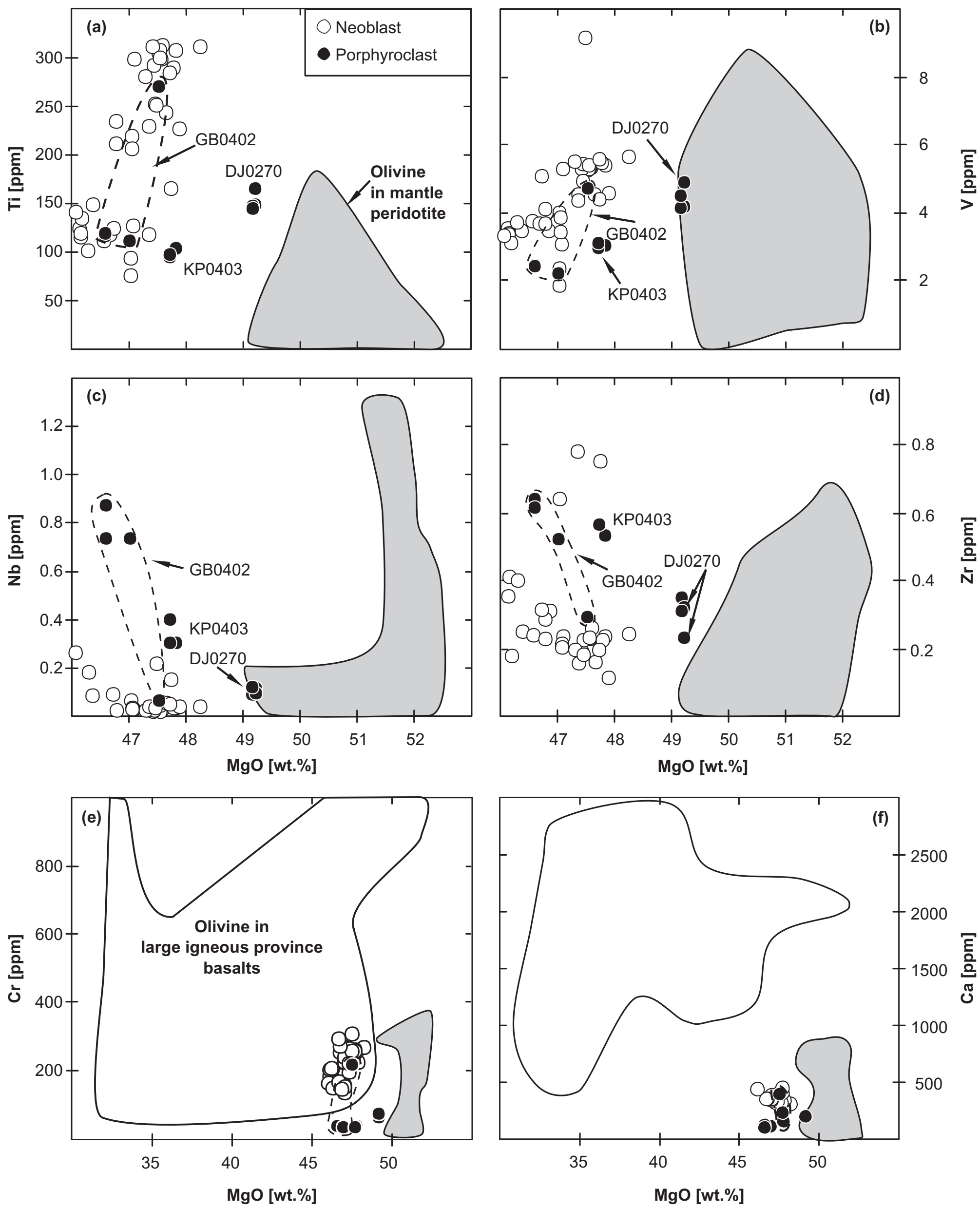

Fig. 7. Trace element composition: (a) Ti, (b) V, (c) Nb, (d) Zr, (e) Cr and (f) Ca vs MgO (wt %) of olivine neoblasts and porphyroclasts in comparison with olivine from mantle peridotites (grey field; Grégoire *et al.*, 2000, 2001; van Achterbergh, 2004) and olivine from large igneous province basalts [white field in (e) and (f); Etendeka: Gibson *et al.*, 2000; Thompson *et al.*, 2001]. [Note different scales in (e) and (f).] Dashed line represents compositional variation in porphyroclast rims in GB0402.

metasomatized, resulting in enrichment of the rocks in Ti, Fe, K, light rare earth elements (LREE) and other large ion lithophile elements (LILE) (Menzies *et al.*, 1987). This metasomatic overprint can change the chemical composition of the primary minerals (cryptic metasomatism; Dawson, 1984) and, at higher degrees of metasomatism, change the modal composition of a rock (modal metasomatism; Harte, 1983) by adding phlogopite and amphibole (e.g. Carswell, 1975; Winterburn *et al.*, 1990), ilmenite and rutile (Mitchell, 1973; Harte *et al.*, 1987), and/or pyroxene and garnet (e.g. Hawkesworth *et al.*, 1990; Simon *et al.*, 2002, 2003; Grégoire *et al.*, 2003) that grow at the expense of the primary minerals.

The exact composition of these metasomatizing agents is highly debated, as is their nature (melt or fluid) and the timing of metasomatism (Erlank *et al.*, 1987). Often a combination of metasomatic fluids and melts of different compositions are proposed, resulting from fractionation of the

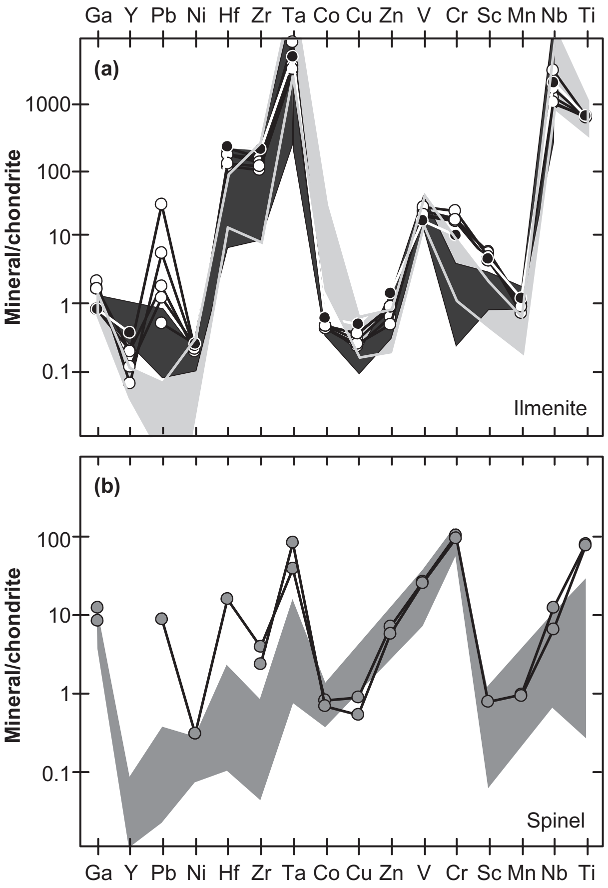

Fig. 8. Chondrite-normalized (McDonough & Sun, 1995) trace element pattern of average oxide compositions in Fe-rich dunite xenoliths: (a) ilmenites: Type I ilmenite (○) and Type II ilmenite (●) are plotted together with mantle-derived ilmenites in eclogites and garnet pyroxenites (black field; Zack & Brumm, 1998; Barth *et al.*, 2002) and megacryst ilmenite from South African kimberlites and the Grib kimberlite (grey field; Kostrovitsky *et al.*, 2004, and references therein); (b) spinel in paragenesis with ilmenite is compared with spinel from abyssal peridotites (grey field) (Grégoire *et al.*, 2000, 2001; Moine *et al.*, 2001).

original metasomatizing agent (Dawson & Smith, 1977; Stachel *et al.*, 1998; Moine *et al.*, 2001) or from different episodes of metasomatism (Dawson, 1984; Carlson *et al.*, 1999; Griffin *et al.*, 2003). In the case of the Kimberley kimberlite cluster, a range of metasomatizing processes related to late Archaean subduction (Griffin *et al.*, 1999; Simon *et al.*, 2003, 2007; Schmitz *et al.*, 2004; van Achterbergh, 2004), Mesozoic Karoo basalt magmatism (Erlank *et al.*, 1980; Hawkesworth *et al.*, 1990; Griffin *et al.*, 2003), and later Cretaceous kimberlite events (Dawson, 1987; Konzett *et al.*, 2000; Grégoire *et al.*, 2003; Simon *et al.*, 2003, 2007) have been suggested.

Kimberlite infiltration leads to enrichment in incompatible trace elements and MgO in the whole-rock. Additionally, post-emplacement weathering and reaction with percolating groundwater results in serpentinitization of olivine rims (average 10 vol. % serpentine in the Fe-rich dunite xenoliths). The analysis of unmetasomatized primary minerals for major and trace elements often helps to see through the metasomatic overprint and the effect of kimberlite infiltration (Barth *et al.*, 2001). In the Fe-rich dunite xenoliths, secondary minerals that are not related to near-surface alteration, such as ilmenite and phlogopite, make up only 1–2·5% of the whole-rock (Table 1), which is much less than typical for metasomatized peridotite xenoliths from the same area (Erlank *et al.*, 1987), so that thorough modification of all trace elements in the remaining 98% of the rock is unlikely.

Metasomatic phases are ilmenite, which occurs in all samples and replaces chromite, and phlogopite, which has been found in three samples. In contrast, serpentine is related to weathering of the kimberlite. The elevated TiO_2 contents in chromite and phlogopite and the metasomatic nature of ilmenite and phlogopite in the Fe-rich dunites document both a modal as well as cryptic metasomatic overprint. If all ilmenites replace spinel, most dunite xenoliths would have had ~1% primary spinel, probably with slightly lower Cr-number than analyzed. The high modal content of olivine argues that its uniform Mg-number is unlikely to result from metasomatic alteration from an originally higher Mg-number. The high Ti contents in olivine, however, might indicate cryptic metasomatism by equilibration with a Ti-rich percolating melt (not the host kimberlite, as it is low in TiO_2; Le Roex *et al.*, 2003).

The timing of the metasomatism is difficult to constrain, but it must have taken place before kimberlite entrainment. Type I ilmenites probably crystallized from a Ti- and Fe-rich melt as commonly proposed to cause Fe–Ti-rich metasomatism in peridotites of the Kaapvaal Craton. Their Cr-rich composition and distinction in trace elements from megacrystic ilmenites (Fig. 8a) may be due to the involvement of spinel in their formation. In contrast, the lower Cr, V and Sc contents of Type II ilmenites may be explained by a similar origin from Fe–Ti-rich melts, but lacking reaction with pre-existing spinel. Konzett *et al.* (2000) demonstrated that zircons in MARID xenoliths from this area crystallized immediately before kimberlite eruption. Despite their contrasting mineralogy, MARID xenoliths may be related to the metasomatic reactions in peridotite described by Erlank *et al.* (1987), as these also produce K-richterite as an end-product. The metasomatism experienced by the dunite xenoliths is possibly related to this event. The deformation documented by foliation along which olivine porphyroclasts and ilmenites are aligned, and which led to recrystallization of the olivines as neoblasts, is temporally related to the metasomatism. This is indicated by zonation of the porphyroclasts towards compositions of neoblasts, which are themselves recrystallized during the deformation.

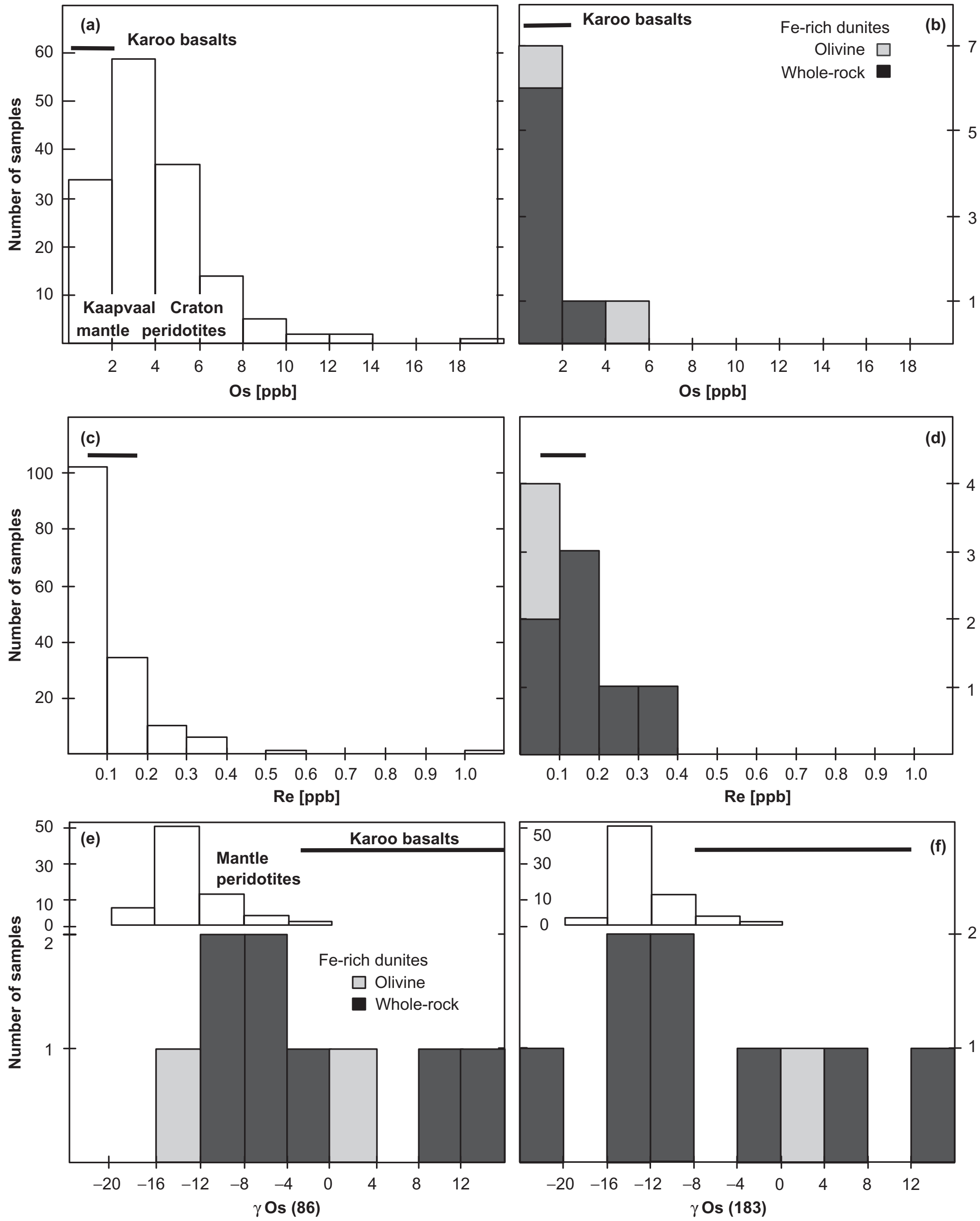

Fig. 9. Re–Os systematics of whole-rock and olivine separates of Fe-rich dunites (b, d, e and f), Karoo basalts (horizontal lines; Ellam *et al.*, 1992) and Kaapvaal mantle peridotites (a, c, e and f; Walker *et al.*, 1989; Pearson *et al.*, 1995*b*; Carlson *et al.*, 1999; Menzies *et al.*, 1999; Irvine *et al.*, 2001; Meisel *et al.*, 2001; Carlson & Moore, 2004; Simon, 2004): (a) and (b) histograms of Os content; (c) and (d) histogram of Re content; (e) histogram of γOs at the time of kimberlite eruption (86 Ma); (f) histogram of γOs at the time of Karoo basalt magmatism (183 Ma).

Origin of the dunite xenoliths—residual mantle, cumulates, or reaction channels

Possible origins for the dunite xenoliths include: (1) residua of peridotite melting in the mantle after removal of a high melt fraction and elimination of clinopyroxene and othropyroxene; (2) reaction products produced by removal of pyroxenes during reaction with percolating melts, as has been described from ophiolites (Kelemen *et al.*, 1992); (3) liquidus cumulates from picritic melts that crystallized in the upper mantle or crust, probably along the walls of cracks through which the melt moved. We restrict ourselves in this discussion to the chemical features that pre-date metasomatism. The texture of the dunite xenoliths is associated with the metasomatic event, probably immediately

Table 4: Re and Os isotope composition of Fe-rich dunite whole-rock samples and olivine separates

Sample: Comment:	AJE410 WR	AJE410 olivine	DJ0267 WR	DJ0268 WR	DJ0269 WR	DJ0270 WR	GB0402 WR	GB0402 olivine	KP0403 WR
Re (ppb)	0·01720	0·00760	0·16840	0·10420	0·22240	0·10590	0·01110	0·00800	0·31540
Os (ppb)	0·12410	0·06770	0·91330	0·06400	0·04450	0·09560	3·38050	4·32910	0·68210
^{187}Re/^{188}Os	0·67180	0·53870	0·88890	7·83750	24·10740	5·33450	0·01590	0·00890	2·23330
2σ error	0·01980	0·07850	0·00320	0·07190	0·27620	0·03760	0·00070	0·00120	0·00420
^{187}Os/^{188}Os	0·14790	0·13470	0·12590	0·13370	0·15160	0·12660	0·11440	0·11340	0·14380
2σ error	0·00011	0·00067	0·00003	0·00032	0·00027	0·00026	0·00001	0·00002	0·00002
^{187}Os/^{188}Os (86)	0·14694	0·13393	0·12463	0·12246	0·11704	0·11895	0·11438	0·11339	0·14060
γOs (86)	13·93	3·84	−3·37	−5·05	−9·26	−7·77	−11·32	−12·09	9·01
^{187}Os/^{188}Os (183)	0·14585	0·13306	0·12319	0·10977	0·07789	0·11031	0·11435	0·11337	0·13698
γOs (183)	13·70	3·73	−3·96	−14·42	−39·20	−14·00	−10·85	−11·61	6·79
T_{RD} (Ga)	−2·44	−0·60	0·68	0·98	1·71	1·45	2·06	2·19	−1·54
2σ error	0·21	0·24	0·11	0·14	0·12	0·12	0·07	0·07	0·17
T_{MA} (Ga)	4·47	2·89	−0·49	0·03	0·05	−0·04	2·14	2·24	0·47
2σ error	0·33	1·25	−0·13	−0·004	0·001	−0·01	0·07	0·06	−0·02

WR, whole-rock. Re-depletion ages (T_{RD}), model ages (T_{MA}) and γOs were calculated according to Walker *et al.* (1989), using present-day Bulk Silicate Earth (BSE) values of ^{187}Os/^{188}Os$_{BSE}$ = 0·1296 and ^{187}Re/^{188}Os$_{BSE}$ = 0·4353 (Meisel *et al.*, 2001). The ^{187}Os/^{188}Os(t) and γOs(t) ratios are age-corrected to a mean Kimberley kimberlite eruption age of 86 ± 3 Ma and a Karoo eruption age of 183 ± 1 Ma.

before eruption of the kimberlite, and consequently provides little information on the processes responsible for initial dunite formation.

Are dunite xenoliths residual after high degrees of melting of peridotite?

The following geochemical features of the dunite xenolith samples contradict an origin as metasomatized mantle peridotites that had previously experienced extensive melt removal. These are: (1) olivine neoblasts that have lower forsterite contents (Fo_{87-89}) than would be expected for a restitic dunite (Fo_{93-95}; Gurney & Harte, 1980); advocating later lowering of the Mg-number by Fe–Ti metasomatism is unreasonable, as this process would need to homogenize 98% of the rock and none of the original Os isotope signal would survive; (2) low Ni contents compared with typical mantle peridotites (Fig 4), which could be expected to be even higher after substantial melt loss because of the high D_{Ni} for olivine–melt pairs (Hart & Davis, 1978); (3) the range in γOs (86 Ma) of −12 to 14 is large compared with mantle xenoliths from the Kaapvaal craton, which have γOs (86 Ma) mostly below −12 (Fig. 9e). The main carrier phases of Os in the mantle are sulphides and alloys, which break down during mantle melting. Hence, although these signatures could be interpreted to reflect melt extraction exceeding the point of sulphide or alloy breakdown, the Re/Os ratios of all dunites except GB0402 are higher than those of primitive mantle, which implies interaction with a high Re/Os ratio melt, such as basalt or kimberlite. The Re–Os data thus provide a strong argument that the majority of the Fe-rich dunites are not simply residua of extensive melt extraction in the Archaean, the explanation commonly applied to the origin of Kaapvaal harzburgites and lherzolites. The high Cr-number of spinels could be taken to be evidence for a restitic origin (Kurat *et al.*, 1980), but these compositions might not be a true reflection of the original composition of the spinels as a result of metasomatic interaction. Furthermore, on account of their high TiO_2, these spinels are not similar to Cr–Al spinels typical of peridotites.

There are few trace element analyses of olivine in peridotites available for a systematic comparison to the trace element data reported here, so that the field for 'mantle peridotites' in Fig. 7 should be treated with some caution until more analyses are available. Some pointers can nevertheless be found: if the dunites originate as residua after high degrees of melt loss from peridotite, then the major and trace element compositions of their olivines must correspond to clinopyroxene-undersaturated conditions. Foley *et al.* (2006) studied trace elements in olivines from Antarctica and described differences between rocks saturated in clinoyproxene (lherzolite) and those that were not. Apart from the expected low Ca contents, olivines from the harzburgitic population have lower

Ti (<35 ppm, mostly <10 ppm), V (<2 ppm), Cr (<60 ppm) and Zn (average 20 ppm) concentrations than those from the lherzolitic population. Olivines in the dunite xenoliths from Kimberley have concentrations of these elements that are much higher than in the Antarctic harzburgites and correspond more closely to the lherzolitic population. There is thus no indication that the olivines originated as components of strongly depleted members of the peridotite suite.

Do dunite xenoliths correspond to reaction products between peridotite and percolating melts?

Many descriptions of dunites in the mantle sections of ophiolites attribute their formation to a reaction process resulting in removal of orthopyroxene by reaction with percolating melts (Kelemen *et al.*, 1992; Suhr *et al.*, 1998). Several points can be used to argue against such an origin for the Fe-rich dunite xenoliths at Kimberley.

(1) Olivines in ophiolitic dunite channels have Mg-number and Mg–Ni characteristics within the mantle array, similar to Kaapvaal mantle peridotites (Fig. 4).

(2) The Re–Os signal should reflect the *in situ* budget of peridotitic material diluted by the signal from the percolating melt. In the mantle sections of ophiolite complexes, harzburgite has higher Os, but lower Re contents than dunite channels and the initial Os isotope ratio of harzburgite is more unradiogenic than that of the dunites (Büchl *et al.*, 2002; Hanghøj *et al.*, 2004). The Kaapvaal dunite xenoliths have similar to slightly less radiogenic initial Os isotope composition compared with ophiolitic dunites (0·1144–0·1469 vs 0·1245–0·1477, respectively), whereas the Re and Os contents of the dunite xenoliths are lower than in ophiolitic channel dunites (0·1 ±0·1 ppb Re and mostly <1 ppb Os). Becker *et al.* (2006) calculated that melt/rock ratios up to 400 were required to remove 50–70% of the osmium from a peridotite by this process. Reduction of Os contents from the 3·5–5·5 ppb Os typical of peridotite (Becker *et al.*, 2006) to <1 ppb in Kimberley dunite olivines requires unrealistically high melt/rock ratios (Becker *et al.*, 2001; Hanghøj *et al.*, 2004).

(3) The reaction channel mechanism is documented for low-pressure oceanic lithosphere settings in which low-SiO_2 melts react with peridotite as a result of the pressure contrast between the depth of origin of the melt and the reaction location. In the case of the dunite xenoliths from Kimberley, formation of dunite in reaction channels would occur within the thick continental lithosphere, where this pressure contrast is unlikely to be so great.

(4) Dunite xenoliths from ocean island basalts (e.g. Hawaii, Kerguelen) have olivine with lower forsterite contents and similar major element and transitional metal element compositions to olivine neoblasts in the dunite xenoliths from Kimberley (Grégoire *et al.*, 2000; Moine *et al.*, 2001). These xenoliths have been ascribed either to crystallization in conduits of the ascending basaltic magma (Kerguelen; Grégoire *et al.*, 2000) or to accumulation in magma chambers (Hawaiian dunites; Clague, 1988; Clague & Bohrson, 1991; Gaffney, 2002). However, trace element analyses of these dunite xenoliths are not available, so that a thorough assessment of similarities to and differences from the Kimberley dunites cannot be made.

Are dunite xenoliths liquidus cumulates of Karoo picrite–basalt?

An origin of Kimberley dunite xenoliths as cumulates is compatible with the similarity of the olivine compositions to olivine megacrysts in Karoo picrites (Fo_{82-92}) and in kimberlites (Fo_{80-88}), both of which are believed to be of cumulate origin (Boyd, 1974; Cox & Jamieson, 1974; Dawson *et al.*, 1981; Schulze, 1987; Nowell *et al.*, 2004). Chromites with Cr-number up to 0·74, at the lower end of the range for spinel in the dunite xenoliths (0·67–0·97), are known from Karoo basalts and are interpreted as cumulate minerals (Eales, 1979). Furthermore, they have high TiO_2 contents of 0·4–9·2 wt %, offering an explanation for the high TiO_2 content of spinel in the Fe-rich dunites. The Re and Os isotope compositions of the most Fe-rich dunite xenoliths have similar Os evolution trends to the Karoo basalts (Fig. 10; Ellam *et al.*, 1992), yielding Re/Os ages of 30 Ma to 1·5 Ga (Table 4), which overlap with Re/Os ages obtained for Karoo basalts (Duncan *et al.*, 1997). Although apparently at odds with an origin as cumulates, sheared textures have been described for megacrysts from kimberlites that are also interpreted as cumulates. This kind of deformation in kimberlite megacrysts has been attributed to deformation within the thermal aureole of the host kimberlite (Moore & Belousova, 2005).

Several lines of evidence suggest that the olivine porphyroclasts may be remnants of much earlier (probably Archaean) cumulate wall rocks, which were incorporated into, or strongly interacted with, the melt from which the olivine neoblasts crystallized. Compared with olivine neoblasts, the porphyroclasts have slightly higher forsterite contents (Fo_{87-91}) and different trace element compositions (Fig. 7). The observation of slight chemical variation towards neoblast composition from porphyroclast core to rim in sample GB0402 (Table 2, Fig. 7) indicates progressive equilibration between the magma and the incorporated wall-rock. Sample DJ0270 has olivine porphyroclasts with V and Nb concentrations that plot within the compositional field of olivine in mantle peridotites. However, the low Ni content of olivine

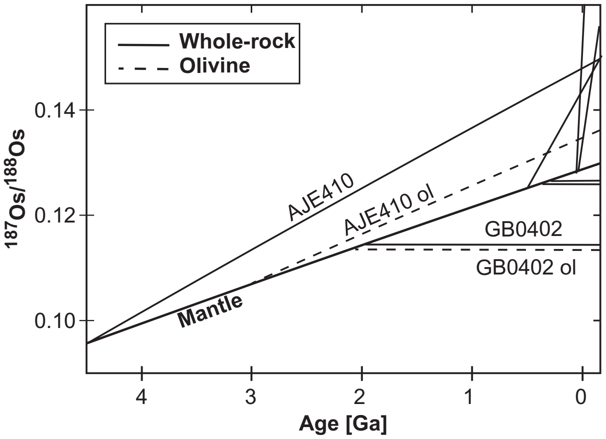

Fig. 10. ^{187}Os/^{188}Os vs time evolution diagram for whole-rocks and olivine separates of Fe-rich dunite xenoliths.

porphyroclasts (1300 ppm) precludes an origin for the porphyroclasts as peridotitic olivines. The porphyroclasts with low Ni contents are best explained as liquidus crystallization products from a slightly fractionated Mg-rich melt, and thus also as cumulates from a magmatic event. However, the Re–Os isotope data require that this 'porphyroclast event' occurred much earlier, possibly during Archaean times. Such an Archaean event might correspond to the Ventersdorp magmatism, whose surface expression comprises basaltic komatiites, basalts, basaltic andesites, andesites and felsic volcanic rocks (Crow & Condie, 1988). The lower Ca content of olivine porphyroclasts compared with olivine neoblasts indicates that the olivine porphyroclasts crystallized at slightly higher pressures (Köhler & Brey, 1990). This may indicate incorporation of the older porphyroclast cumulate component from lower lithospheric levels during ascent of the Karoo magma and crystallization of olivine neoblasts at higher levels.

The Os isotope compositions place some constraints on the origin of the high Re/Os ratio of the majority of the Fe-rich dunites. Using the measured Re/Os ratios of the samples and correcting back to the eruption age of the host kimberlite (86 Ma), the Os isotope composition of the dunites ranges from significantly higher than estimates for primitive mantle [i.e. samples AJE410 and KP0403 with γOs (86 Ma) between +4 and +14] through values slightly lower than primitive mantle [samples DJ0267, DJ0268, DJ0269 and DJ0270 with γOs (86 Ma) $= -3$ to -9], to sample GB0402 with an Os isotope composition approaching that typical for Kaapvaal peridotites ($-12{\cdot}5 \pm 0{\cdot}2$; Fig. 9e). If corrected back to the ~183 Ma eruption age of the Karoo basalts (Duncan *et al.*, 1997), however, samples DJ0268 and DJ0270 would have Os isotope compositions within the range of most Kaapvaal peridotites, whereas sample DJ0269, with the highest Re/Os of the dataset, would have unrealistically low ^{187}Os/^{188}Os ratio, below that of the initial ^{187}Os/^{188}Os of the Earth (Fig. 9f; Table 4). Clearly, for samples DJ0268, DJ0269 and DJ0270, the high Re/Os ratio must be a fairly recent (i.e. Phanerozoic) phenomenon. If the dunites formed during the Karoo event and their Re/Os ratios were not significantly perturbed by infiltration by the host kimberlite, then the low ^{187}Os/^{188}Os at 183 Ma of samples DJ0268, DJ0270 and GB0402, are compatible with the suggestion that the dunites formed from interaction between Karoo melts and pre-existing ancient lithosphere. Sample GB0402 has the lowest Re/Os and ^{187}Os/^{188}Os of all Fe-rich dunites, suggesting that the bulk of the Os is derived from an Archaean source consistent with the high modal abundance of porphyroclastic olivine. Hence, although most samples seem to have originated from Phanerozoic (Karoo) magmas, the preserved porphyroclasts and the Re–Os isotope systematics of samples DJ0268, DJ0270 and GB0402 show evidence for incorporation of Archaean (possibly Ventersdorp) cumulate material, which may indicate reactivation of old melt channels.

The unrealistically low ^{187}Os/^{188}Os calculated for sample DJ0269 at 183 Ma, however, indicates modification of the Re–Os system more recently than Karoo volcanism, and the likely candidate here is infiltration of the xenoliths by their host kimberlite. The significant difference in Os isotope composition between the olivine separate and whole-rock for sample AJE410, and the presence of ilmenite in KP0403 with similar Os isotope characteristics to AJE410, provide additional evidence that interaction with the host kimberlite indeed played a role in modifying the composition of these three dunites.

Picrite fractionation and dunite crystallization conditions

From the above discussion, an origin of most dunite xenoliths as metasomatically modified and deformed liquidus cumulates from picrite–basalt melts of the Karoo period appears most likely. To further evaluate this hypothesis, we calculated the parental magma compositions for olivines in the dunites and compared them with primitive basalt compositions from the southern low-Ti Karoo basalt province (Fig. 1) from which the dunites may have crystallized. This hypothetical parental magma is calculated from the olivine composition, using published crystal–melt partition ($D_{\mathrm{liq}}^{\mathrm{ol}} = X_{\mathrm{element}}^{\mathrm{ol}}/X_{\mathrm{element}}^{\mathrm{liq}}$) and distribution coefficients [$K_{\mathrm{D}} = (X_{\mathrm{oxide1}}^{\mathrm{ol}}/X_{\mathrm{oxide2}}^{\mathrm{ol}})/(X_{\mathrm{oxide1}}^{\mathrm{liq}}/X_{\mathrm{oxide2}}^{\mathrm{liq}})$]. The olivine compositions were assumed to represent pre-metasomatic chemistry (i.e. Mg-number was not lowered during metasomatism): the Mg-numbers calculated for coexisting melts are thus minimum values. The olivine neoblasts have FeO/MgO ratios of 0·22–0·27, corresponding to a coexisting melt composition with FeO/MgO of 0·69–0·89 using a K_{D} of 0·30 (Roeder & Emslie,

Table 5: Parental magma composition (wt %) calculated from olivine trace element compositions in Table 2 and literature partition coefficients $D_{ol/liq}$, compared with primitive low-Ti Karoo basalts

Sample:	AJE410 nb	DJ0267 nb	DJ0268 nb	DJ0269 nb	DJ0270 pc	DJ0270 nb	GB0402 pc	GB0402 nb	KP0403 pc	KP0403 nb	Karoo range	$D_{ol/liq}$ ref.
FeO/MgO	0·89	0·83	0·83	0·69	0·58	0·72	0·88	0·89	0·82	0·84	0·46–2·40	1
MgO	11·84	12·67	12·90	14·43	18·00	14·68	11·92	11·75	12·78	12·53	4·70–31·49	1
SiO_2	43·62	43·81	44·85	43·75	44·00	43·56	44·57	44·49	44·25	44·39	42·46–53·80	2
TiO_2	0·89	0·80	2·22	2·36	1·32	1·88	0·82	1·48	0·72	1·30	0·41–2·40	3
Al_2O_3	3·73	1·58	7·73	–	2·08	7·00	–	–	–	–	5·97–16·49	4
CaO	6·06	–	7·39	7·63	3·69	6·37	4·86	8·42	17·38	10·80	4·36–12·60	5
Cr_2O_3	0·11	0·09	0·13	0·14	0·04	0·13	0·03	0·14	0·02	0·16	–	6
MnO	0·07	0·07	0·09	0·12	0·07	0·07	0·18	0·13	0·11	0·09	0·15–0·25	7
NiO	0·03	0·04	0·04	0·06	0·04	0·04	0·02	0·05	0·02	0·05	–	8

Abbreviations as in Tables 1 and 2. Primitive low-Ti Karoo basalts from Cox *et al*. (1967), Eales & Marsh (1979) and Cox (1983, 1988). References for partition coefficients: 1, Roeder & Emslie (1970); 2, Beattie *et al*. (1991); 3, Bédard (2005); 4, Colson *et al*. (1988); 5, Higuchi & Nagasawa (1969); 6, Ohtani *et al*. (1989); 7, Dunn (1987); 8, Hart & Davis (1978).

1970), and lie within the lower part of the FeO/MgO range of primitive low-Ti Karoo basalt (0·39–2·38; Cox *et al*., 1967; Cox 1983; Marsh *et al*., 1997). Olivine porphyroclasts have FeO/MgO ratios of 0·18–0·27, corresponding to FeO/MgO ratio of the coexisting melt of 0·58–0·88. The parental melts calculated for olivine porphyroclasts have lower FeO/MgO ratios than for the coexisting olivine neoblasts, indicating a higher MgO content (Table 5), which is consistent with the basal section of the Ventersdorp Klipriviersberg Group comprising high-Mg and komatiitic rocks progressing to later tholeiitic basalts (e.g. Crow & Condie, 1988; Eriksson *et al*., 2002). This is consistent with the interpretation that the olivine porphyroclasts are remnants of an initially more magnesian, but slightly fractionated melt, explaining their lower Ni contents. Following the procedure of Eales & Marsh (1979), and using a total iron content (as $Fe_2O_3^*$) of 11·6 wt % (average low-Ti Karoo basalt) and a Fe_2O_3/FeO ratio of 0·20 (Brooks, 1976) we recalculated the iron and magnesium content of the parental melt of the olivine neoblasts and porphyroclasts (Table 5). The most primitive olivine neoblasts have a parental melt composition with Fe_2O_3 2·1 wt %, FeO 10·5 wt % and MgO 15·3 wt %. Additionally, it is possible to calculate concentrations of SiO_2, CaO, NiO, MnO, Cr_2O_3, Al_2O_3 and TiO_2 in the parental melt using experimental and naturally determined olivine–basalt melt partition coefficients. The predicted TiO_2 content of the parental magmas is 0·7–2·4 wt % and lies within the TiO_2 range of primitive low-Ti Karoo basalts (0·4–2·4 wt %). The calculated parental magma composition lies within the range of primitive low-Ti Karoo basalt composition for all major elements (Table 5). This observation, together with the high MgO content of the parental magma, supports the interpretation that the Fe-rich dunites are cumulates from low-Ti Karoo picrites that erupted in the same area in Jurassic times (Fig. 1).

To test this hypothesis and to reproduce the Fe-rich dunite olivine composition, we modelled the fractional crystallization of the calculated parental picrite melt of the most primitive olivine neoblast with pMELTS (Ghiorso & Hirschmann, 1998), which uses the same olivine–melt FeO–MgO distribution coefficient of 0·30 used in calculating the parental magma composition (Ghiorso & Sack, 1995). Fractional crystallization was modelled isobarically (10 kbar) in temperature intervals of 1°C, beginning at the liquidus calculated by pMELTS (~1400°C). Because Karoo basalts are hydrous, with water contents of 0·5–2·6 wt % (Eales & Marsh, 1979) olivine fractionation was modelled under hydrous conditions (2% water). This yielded 15% olivine fractionation and led towards more tholeiitic melt compositions. Subsequently, spinel and clinopyroxene crystallize from the melt. The modelled fractional crystallization shows similar oxide variation to that seen in the primitive basalts of low-Ti Karoo basalts (Table 5) and other large igneous provinces worldwide. At similar forsterite contents, olivine fractionating from the parental melt in equilibrium with the most primitive olivine porphyroclasts has lower NiO (0·1–0·2 wt %), MnO (0·2 wt %) and CaO (0·3 wt %) contents than olivine from the neoblast parental melt, which agrees well with the composition of the olivine porphyroclasts. The NiO content of the modelled olivine overlaps with the composition of olivine in the Fe-rich dunite xenoliths (NiO 0·3–0·8 wt %), whereas MnO and CaO are slightly overestimated (0·5 and 0·3–0·4 wt %, respectively). The calculated parental melt of the most primitive olivine porphyroclasts has lower Al_2O_3, TiO_2 and CaO and higher SiO_2 fractionation trends (modelled hydrous, at 10 kbar with pMELTS). This is similar to the composition of Ventersdorp volcanic rocks, which also have higher SiO_2 and lower Al_2O_3, TiO_2 and CaO contents than low-Ti Karoo basalts (Crow & Condie, 1988; Marsh *et al.*, 1989).

CONCLUSIONS

Fine-grained Fe-rich dunite xenoliths from South African kimberlites have minerals with major and trace element compositions differing from those in mantle peridotites. Their low forsterite and NiO contents as well as low Os content and high Re/Os and $^{187}Os/^{188}Os$ ratios contradict an origin as restite after melting of peridotite, but are strong evidence for an origin as recrystallized magmatic cumulates. Modelling of fractional crystallization from estimated parental magma composition with pMELTS yields up to 15% olivine fractionation followed by spinel and clinopyroxene crystallization, which drives the melt compositions towards tholeiitic compositions. The composition of the fractionating olivine is similar to that of olivine in the Fe-rich dunites. Modelled element fractionation trends successfully reproduce the compositional variation of large igneous province basalts. In contrast, olivine porphyroclasts have higher Fo and lower NiO contents than olivine neoblasts, showing that these are remnants of cumulates from different, much earlier magmatic episodes. Re–Os isotope systematics indicate an Archaean age for these porphyroclasts. The petrogenetic history of the Fe-rich dunites can be summarized as follows.

(1) ~2·7 Ga: fractional crystallization and accumulation of olivine from an Archaean (probably Ventersdorp) komatiite–picrite melt, indicated by low $^{187}Os/^{188}Os$ at 183 Ma, and now present as olivine porphyroclasts.

(2) 183 Ma: Karoo magmatism results in formation of olivine cumulates carrying the Re–Os signature of low-Os melts at this time. Abundant olivine crystallization, now represented by the neoblast population, is accompanied by minor spinel crystallization (1–2%). The rare porphyroclasts in the dunites are incorporated from event (1) torn out by reactivation of Archaean veins.

(3) ~90–86 Ma: metasomatic overprinting of the dunites, resulting in reaction of spinel to form Type I ilmenite ± phlogopite, and readjustment of the Re–Os system. Deformation occurred at about the same time, resulting in growth of neoblasts and elimination of earlier textures. Only the largest porphyroclasts remain intact from earlier episodes. This event corresponds to the zircon ages in MARID xenoliths from the same area (Konzett *et al.*, 2000).

(4) 86 Ma: incorporation into the kimberlite melt.

ACKNOWLEDGEMENTS

Samples were collected by D.E.J. and provided to us by the University of Cape Town (A. J. Erlank collection) and by G. P. Brey (J. W. Goethe University, Frankfurt). J. Robey (DeBeers, Kimberley) provided expert assistance in collecting xenoliths. The help of the laboratory managers B. Schulz-Dobrick and M. G. Barth (Mainz University), D. Lowry (Royal Holloway University of London), M. Horan and T. D. Mock (Carnegie Institution of Washington) is gratefully acknowledged. The manuscript was improved by helpful comments of the two reviewers Hilary Downes and Nina Simon. This project was financially supported by the Deutsche Forschungsgemeinschaft (Fo181/17-1).

REFERENCES

Allsopp, H. L. & Barrett, D. R. (1975). Rb–Sr age determinations on South African kimberlite pipes. *Physics and Chemistry of the Earth* **9**, 605–617.

Arai, S. (1994). Characterization of spinel peridotites by olivine–spinel compositional relationships: review and interpretation. *Chemical Geology* **113**, 191–204.

Armstrong, A. (1995). CITZAF—a package of correction programs for the quantitative electron microbeam X-ray-analysis of thick polished materials, thin-films, and particles. *Microbeam Analysis* **4**, 177–200.

Barth, M. G., Rudnick, R. L., Horn, I., McDonough, W. F., Spicuzza, M. J., Valley, J. W. & Haggerty, S. E. (2001). Geochemistry of xenolithic eclogites from West Africa, Part I: a link between low MgO eclogites and Archean crust formation. *Geochimica et Cosmochimica Acta* **65**, 1499–1527.

Barth, M. G., Rudnick, R. L., Horn, I., McDonough, W. F., Spicuzza, M. J., Valley, J. W. & Haggerty, S. E. (2002). Geochemistry of xenolithic eclogites from West Africa, part 2: origins of the high MgO eclogites. *Geochimica et Cosmochimica Acta* **66**, 4325–4345.

Beattie, P., Ford, C. & Russell, D. (1991). Partition coefficients for olivine–melt and orthopyroxene–melt systems. *Contributions to Mineralogy and Petrology* **109**, 212–224.

Becker, H., Shirey, S. B. & Carlson, R. W. (2001). Effects of melt percolation on the Re–Os systematics of peridotites from a Paleozoic convergent plate margin. *Earth and Planetary Science Letters* **188**, 107–121.

Becker, H., Horan, M. F., Walker, R. J., Gao, S., Lorand, J.-P. & Rudnick, R.L. (2006). Highly siderophile element composition of the Earth's primitive upper mantle: constraints from new data on peridotite massifs and xenoliths. *Geochimica et Cosmochimica Acta* **70**, 4528–4550.

Bédard, J. H. (2005). Partitioning coefficients between olivine and silicate melts. *Lithos* **83**, 394–419.

Boyd, F. R. (1974). Olivine megacrysts from the kimberlite of the Monastery and Frank Smith kimberlite pipe, South Africa. *Carnegie Institution of Washington Yearbook* **73**, 282–285.

Boyd, F. R. (1989). Compositional distinction between oceanic and cratonic lithosphere. *Earth and Planetary Science Letters* **96**, 15–26.

Boyd, F. R. & Nixon, P. H. (1975). Origins of the ultramafic nodules from some kimberlites of northern Lesotho and the Monastery mine, South Africa. *Physics and Chemistry of the Earth* **9**, 431–454.

Boyd, F. R., Jones, A. P. & Nixon, G. T. (1983). Mantle metasomatism: the Kimberley dunites. *Carnegie Institution of Washington Yearbook* **83**, 330–337.

Brooks, C. K. (1976). The Fe_2O_3/FeO ratio of basalt analyses: an appeal for a standardized procedure. *Bulletin of the Geological Society of Denmark* **25**, 117–120.

Büchl, A., Brügmann, G., Batanova, V. G., Münker, C. & Hofmann, A. W. (2002). Melt percolation monitored by Os isotopes and HSE abundances: a case study from the mantle section of the Troodos Ophiolite. *Earth and Planetary Science Letters* **204**, 385–402.

Carlson, R. W. & Moore, R. O. (2004). Age of the Eastern Kaapvaal mantle: Re–Os isotope data for peridotite xenoliths from the Monastery kimberlite. *South African Journal of Geology* **107**, 81–90.

Carlson, R. W., Pearson, D. G., Boyd, F. R., Shirey, S. B., Irvine, G., Menzies, A. H. & Gurney, J. J. (1999). Re–Os systematics of lithospheric peridotites: implications for lithosphere formation and preservation. In: Gurney, J. J., Gurney, J. L., Pascoe, M. D. & Richardon, S. H. (eds) *Proceedings of the 7th International Kimberlite Conference, Volume 1.* Cape Town: Red Roof, pp. 99–108.

Carswell, D. A. (1975). Primary and secondary phlogopites and clinopyroxenes in garnet lherzolite xenoliths. *Physics and Chemistry of the Earth* **9**, 417–429.

Carswell, D. A. & Dawson, J. B. (1970). Garnet peridotite xenoliths in South African kimberlite pipes and their petrogenesis. *Contributions to Mineralogy and Petrology* **25**, 163–184.

Carswell, D. A., Clarke, D. B. & Mitchell, R. H. (1979). The petrology and geochemistry of ultramafic nodules from pipe 200, northern Lesotho. In: Boyd, F. R. & Meyer, H. O. A. (eds) *Kimberlites, Diatremes and Diamonds: Their Geology, Petrology and Geochemistry, Volume 2.* Washington, DC: American Geophysical Union, pp. 127–144.

Clague, D. A. (1988). Petrology of ultramafic xenoliths from Loihi Seamount, Hawaii. *Journal of Petrology* **29**, 1161–1186.

Clague, D. A. & Bohrson, W. A. (1991). Origin of xenoliths in the trachyte at Puu Waawaa, Hualalai Volcano, Hawaii. *Contributions to Mineralogy and Petrology* **108**, 439–452.

Colson, R. O., McKay, G. A. & Taylor, L. A. (1988). Temperature and composition dependencies of trace element partitioning: olivine/melt and low-Ca pyroxene/melt. *Geochimica et Cosmochimica Acta* **52**, 539–553.

Cox, K. G. (1983). The Karoo province of southern Africa: origin of trace element enrichment patterns. In: Hawkesworth, C. J. & Norry, M. J. (eds) *Continental Basalts and Mantle Xenoliths.* Nantwich: Shiva, pp. 139–157.

Cox, K. G. (1988). The Karoo province. In: MacDougall, J. D. (ed.) *Continental Flood Basalts.* Dordrecht: Kluwer, pp. 239–271.

Cox, K. G. & Jamieson, B. G. (1974). The olivine-rich lavas of Nuanetsi: a study of polybaric magmatic evolution. *Journal of Petrology* **15**, 269–301.

Cox, K. G., Macdonald, R. & Hornung, G. (1967). Geochemical and petrographic provinces in the Karroo basalts of southern Africa. *American Mineralogist* **52**, 1451–1474.

Crow, C. & Condie, K. C. (1988). Geochemistry and origin of Late Archean volcanics from the Ventersdorp Supergroup, South Africa. *Precambrian Research* **42**, 19–37.

Davis, D. L. (1977). The ages and uranium contents of zircons from kimberlites and associated rocks. *Carnegie Institution of Washington Yearbook* **76**, 631–653.

Dawson, J. B. (1984). Contrasting types of upper-mantle metasomatism. In: Kornprobst, J. (ed.) *Kimberlites II: the Mantle and Crust–Mantle Relationships.* Amsterdam: Elsevier, pp. 289–294.

Dawson, J. B. (1987). The MARID suite of xenoliths in Kimberlites: relationship to veined and metasomatised peridotite xenoliths. In: Nixon, P. H. (ed.) *Mantle Xenoliths.* Chichester: John Wiley, pp. 465–474.

Dawson, J. B. (2004). A fertile harzburgite–garnet lherzolite transition: possible inferences for the roles of strain and metasomatism in upper mantle peridotites. *Lithos* **77**, 553–569.

Dawson, J. B. & Smith, C. B. (1977). The MARID (mica–amphibole–rutile–ilmenite–diopside) suite of xenoliths in kimberlite. *Geochimica et Cosmochimica Acta* **41**, 309–323.

Dawson, J. B., Hervig, R. L. & Smith, J. V. (1981). Fertile iron-rich dunite xenoliths from the Bultfontein kimberlite, South Africa. *Fortschritte der Mineralogie* **59**, 303–324.

Duncan, R. A., Hooper, P. R., Rehacek, J., Marsh, J. S. & Duncan, A. R. (1997). The timing and duration of the Karoo igneous event, southern Gondwana. *Journal of Geophysical Research* **102**, 18127–18138.

Dunn, T. (1987). Partitioning of Hf, Lu, Ti, and Mn between olivine, clinopyroxene and basaltic liquid. *Contributions to Mineralogy and Petrology* **96**, 476–484.

Eales, H. V. (1979). Anomalous Karroo spinels along the chromite–titanomagnetite join. *South African Journal of Science* **75**, 24–29.

Eales, H. V. & Marsh, J. S. (1979). High-Mg tholeiitic rocks and their significance in the Karroo Central Province. *South African Journal of Science* **75**, 400–404.

Eglington, B. M. & Armstrong, R. A. (2004). The Kaapvaal Craton and adjacent orogens, southern Africa: a geochronological database and overview of the geological development of the craton. *South African Journal of Geology* **107**, 13–32.

Ellam, R. M. & Cox, K. G. (1991). An interpretation of Karoo picrite basalts in terms of interaction between asthenospheric magmas and the mantle lithosphere. *Earth and Planetary Science Letters* **105**, 303–342.

Ellam, R., Carlson, R. & Shirey, S. (1992). Evidence from Re–Os isotopes for plume–lithosphere mixing in Karoo flood basalt genesis. *Nature* **359**, 718–721.

Eriksson, P. G., Condie, K. C., van der Westhuizen, W., van der Merwe, R., de Bruiyn, H., Nelson, D. R., Altermann, W., Catuneanu, O., Bumby, A. J., Lindsay, J. & Cunningham, M. J. (2002). Late Archaean superplume events: a Kaapvaal–Pilbara perspective. *Journal of Geodynamics* **34**, 207–247.

Erlank, A., Allsopp, H., Duncan, A. & Bristow, J. (1980). Mantle heterogeneity beneath southern Africa: evidence from the volcanic record. *Philosophical Transactions of the Royal Society of London* **297**, 295–307.

Erlank, A. J., Waters, F. G., Hawkesworth, C. J., Haggerty, S. E., Allsopp, H. L., Rickard, R. S. & Menzies, M. (1987). Evidence for mantle metasomatism in peridotite nodules from the Kimberley pipes, South Africa. In: Menzies, M. A. & Hawkesworth, C. J. (eds) *Mantle Metasomatism.* London: Academic Press, pp. 221–311.

Foley, S. F., Buhre, S., Jacob, D. & Rehfeldt, T. (2003*a*). Pyroxenite and dunite xenoliths as metamorphosed cumulates from the Archean lower ocean crust. *Extended Abstracts of the 8th International Kimberlite Conference, Victoria*, pp. 1–3.

Foley, S. F., Buhre, S. & Jacob, D. E. (2003*b*). Evolution of the Archaean crust by delamination and shallow subduction. *Nature* **421**, 249–252.

Foley, S. F., Andronikov, A. V., Jacob, D. E. & Melzer, S. (2006). Evidence from Antarctic mantle peridotite xenoliths for changes in mineralogy, geochemistry and geothermal gradients beneath a developing rift. *Geochimica et Cosmochimica Acta* **70**, 3096–3120.

Gaffney, A. M. (2002). Environments of crystallization and compositional diversity of Mauna Loa xenoliths. *Journal of Petrology* **43**, 963–980.

Ghiorso, M. S. & Sack, R. O. (1995). Chemical mass transfer in magmatic processes IV. A revised and internally consistent thermodynamic model for the interpolation and extrapolation of liquid-solid equilibria in magmatic systems at elevated temperatures and pressures. *Contributions to Mineralogy and Petrology* **119**, 197–212.

Ghiorso, M. S. & Hirschmann, M. M. (1998). pMELTS: a revised calibration of MELTS for modelling peridotite melting at high pressure. *EOS Transactions, American Geophysical Union* **79**, F1005.

Gibson, S. A., Thompson, R. N. & Dickin, A. P. (2000). Ferropicrites: geochemical evidence for Fe-rich streaks in upwelling mantle plumes. *Earth and Planetary Science Letters* **174**, 355–374.

Grégoire, M., Moine, B. N., O'Reilly, S. Y., Cottin, J.-Y. & Giret, A. (2000). Trace element residence and partitioning in mantle xenoliths metasomatized by highly alkaline, silicate- and carbonate-rich melts (Kerguelen Islands, Indian Ocean). *Journal of Petrology* **41**, 477–509.

Grégoire, M., McInnes, B. I. A. & O'Reilly, S. Y. (2001). Hydrous metasomatism of oceanic sub-arc mantle, Lihir, Papua New Guinea Part 2. Trace element characteristics of slab-derived fluids. *Lithos* **59**, 91–108.

Grégoire, M., Bell, D. R. & Le Roex, A. P. (2002). Trace element geochemistry of phlogopite-rich mafic mantle xenoliths: their classification and their relationship to phlogopite-bearing peridotites and kimberlites revisited. *Contributions to Mineralogy and Petrology* **142**, 603–625.

Grégoire, M., Bell, D. R. & Le Roex, A. P. (2003). Garnet lherzolites from the Kaapvaal Craton (South Africa): trace element evidence for a metasomatic history. *Journal of Petrology* **44**, 629–657.

Griffin, W. L., Shee, S. R., Ryan, C. G., Win, T. T. & Wyatt, B. A. (1999). Harzburgite to lherzolite and back again: metasomatic processes in ultramafic xenoliths form the Wesselton kimberlite, Kimberley, South Africa. *Contributions to Mineralogy and Petrology* **134**, 232–250.

Griffin, W. L., O'Reilly, S. Y., Natapov, L. M. & Ryan, C. G. (2003). The evolution of lithospheric mantle beneath the Kalahari Craton and its margins. *Lithos* **71**, 215–241.

Gurney, J. J. & Harte, B. (1980). Chemical variations in upper mantle nodules from southern Africa kimberlites. *Philosophical Transactions of the Royal Society of London, Series A* **297**, 273–293.

Gurney, J. J., Moore, R. B., Otter, M. L., Kirkley, M. B., Hops, J. J. & McCandless, T. E. (1991). Southern African kimberlites and their xenoliths. In: Kampunzu, A. B. & Lubala, R. T. (eds) *Magmatism in Extensional Structural Settings*. Heidelberg: Springer, pp. 495–536.

Halter, W. E., Pettke, T., Heinrich, C. A. & Rothen-Rutishauser, B. (2002). Major to trace element analysis of melt inclusions by laser-ablation ICP-MS: methods of quantification. *Chemical Geology* **183**, 63–86.

Hanghøj, K., Hassler, D. & Kelemen, P. B. (2004). Re–Os isotope and PGE systematics of peridotites from the Oman Ophiolite. *Geochimica et Cosmochimica Acta* **68**, A703.

Hart, S. R. & Davis, K. E. (1978). Nickel partitioning between olivine and silicate melt. *Earth and Planetary Science Letters* **40**, 203–219.

Hart, S. R., Blusztajn, J., Dick, H. J. B., Meyer, P. S. & Muehlenbachs, K. (1999). The fingerprint of seawater circulation in a 500-meter section of ocean crust gabbros. *Geochimica et Cosmochimica Acta* **63**, 4059–4080.

Harte, B. (1983). Mantle peridotites and processes—the Kimberlite sample. In: Hawkesworth, C. J. & Norry, M. J. (eds) *Continental Basalts and Mantle Xenoliths*. Nantwich: Shiva, pp. 46–91.

Harte, B., Cox, K. G. & Gurney, J. J. (1975). Petrography and geological history of upper mantle xenoliths from the Matsoku kimberlite pipe. *Physics and Chemistry of the Earth* **9**, 477–506.

Harte, B., Winterburn, P. A. & Gurney, J. J. (1987). Metasomatic and enrichment phenomena in garnet peridotite facies mantle xenoliths from the Matsoku kimberlite pipe, Lesotho. In: Menzies, M. A. & Hawkesworth, C. J. (eds) *Mantle metasomatism*. London: Academic Press, pp. 145–220.

Hawkesworth, C. J., Erlank, A. J., Kempton, P. D. & Waters, F. G. (1990). Mantle metasomatism: isotope and trace-element trends in xenoliths from Kimberley, South Africa. *Chemical Geology* **85**, 19–34.

Higuchi, H. & Nagasawa, H. (1969). Partition of trace elements between rock-forming minerals and the host volcanic rocks. *Earth and Planetary Science Letters* **7**, 281–287.

Hills, D. V. & Haggerty, S. E. (1989). Petrochemistry of eclogites from the Koidu Kimberlite Complex, Sierra Leone. *Contributions to Mineralogy and Petrology* **103**, 397–422.

Irvine, G. J., Pearson, D. G. & Carlson, R. W. (2001). Lithospheric mantle evolution of the Kaapvaal Craton: a Re–Os isotope study of peridotite xenoliths from Lesotho kimberlites. *Geophysical Research Letters* **28**, 2505–2508.

Jacob, D. E. (2004). Nature and origin of eclogite xenoliths from kimberlites. *Lithos* **77**, 295–316.

Jacob, D. E., Schmickler, B. & Schulze, D. J. (2003). Trace element geochemistry of coesite-bearing eclogites from the Roberts Victor kimberlite, Kaapvaal craton. *Lithos* **71**, 337–351.

Jourdan, F., Féraud, G., Bertrand, H., Kampunzu, A. B., Tshoso, G., Le Gall, B., Tiercelin, J. J. & Capize, P. (2004). The Karoo triple junction questioned: evidence from Jurassic and Proterozoic ^{40}Ar/^{39}Ar ages and geochemistry of the giant Okavango dyke swarm (Botswana). *Earth and Planetary Science Letters* **222**, 989–1006.

Kelemen, P. B., Dick, H. J. B. & Quick, J. E. (1992). Formation of harzburgite by pervasive melt/rock reaction in the upper mantle. *Nature* **358**, 635–641.

Koga, K. T., Kelemen, P. B. & Shimizu, N. (2001). Petrogenesis of the crust–mantle transition zone and the origin of lower crustal wehrlite in the Oman ophiolite. *Geochemistry, Geophysics, Geosystems 2* paper number 2000GC000132.

Köhler, T. & Brey, G. P. (1990). Calcium exchange between olivine and clinopyroxene calibrated as a geothermobarometer for natural peridotites from 2 to 60 kb with application. *Geochimica et Cosmochimica Acta* **54**, 2375–2388.

Konzett, J., Armstrong, R. A. & Günther, D. (2000). Modal metasomatism in the Kaapvaal craton lithosphere: constraints on timing and genesis from U–Pb zircon dating of metasomatized peridotites and MARID-type xenoliths. *Contributions to Mineralogy and Petrology* **139**, 704–719.

Kostrovitsky, S. I., Malkovets, V. G., Verichev, E. M., Garanin, V. K. & Suvorova, L. V. (2004). Megacrysts from the Grib kimberlite pipe (Arkhangelsk Province, Russia). *Lithos* **77**, 511–523.

Kubo, K. (2002). Dunite formation processes in highly depleted peridotite: case study of the Icanaidake peridotite, Hokkaido, Japan. *Journal of Petrology* **43**, 423–448.

Kurat, G., Palme, H., Spettel, B., Baddenhausen, H., Hofmeister, H., Palme, C. & Wänke, H. (1980). Geochemistry of ultramafic xenoliths from Kapfenstein, Austria: evidence for a variety of upper mantle processes. *Geochimica et Cosmochimica Acta* **44**, 45–60.

Lee, C.-T. & Rudnick, R. L. (1999). Compositional stratified cratonic lithosphere: petrology and geochemistry of peridotite xenoliths from the Labait Volcano, Tanzania. In: Gurney, J. J., Gurney, J. L., Pascoe, M. D. & Richardson, S. H. (eds) *Proceedings of the 7th International Kimberlite Conference*. Nixon volume. Cape Town: Red Roof, pp. 503–521.

Le Roex, A. P., Bell, D. R. & Davis, P. (2003). Petrogenesis of group I kimberlites from Kimberley, South Africa: evidence from bulk rock geochemistry. *Journal of Petrology* **44**, 2261–2286.

Lowry, D., Appel, P. W. U. & Rollinson, H. R. (2003). Oxygen isotopes of an early Archaean layered ultramafic body, southern West Greenland: implications for magma source and post-intrusion history. *Precambrian Research* **126**, 273–288.

MacGregor, I. D. & Carter, J. L. (1970). The chemistry of clinopyroxenes and garnets of eclogite and peridotite xenoliths from the Roberts Victor mine, South Africa. *Physics of the Earth and Planetary Interiors* **3**, 391–397.

Marsh, J. S., Bowen, M. P., Rogers, N. W. & Bowen, T. B. (1989). Volcanic rocks of the Witwatersrand Triad, South Africa. II: Petrogenesis of mafic and felsic rocks of the Dominion Group. *Precambrian Research* **44**, 39–65.

Marsh, J. S., Hooper, P. R., Rehacek, J., Duncan, R. A. & Duncan, A. R. (1997). Stratigraphy and age of Karoo basalts of Lesotho and implications for correlations within the Karoo igneous province. In: Mahoney, J. J. & Coffin, M. F. (eds) *Large Igneous Provinces: Continental, Oceanic, and Planetary Flood Volcanism*. Washington: American Geophysical Union **100**, 247–272.

Mattey, D. (1997). LaserPrep: an automatic laser-fluorination system for Micromass 'Optima' or 'Prism' mass spectrometers. *Micromass Application Note* **107**, 1–7.

Mattey, D. & Macpherson, C. (1993). High-precision oxygen isotope microanalysis of ferromagnesian minerals by laser-fluorination. *Chemical Geology* **105**, 305–318.

Mattey, D., Lowry, D. & Macpherson, C. (1994). Oxygen isotope composition of mantle peridotite. *Earth and Planetary Science Letters* **128**, 231–241.

McDonough, W. F. & Sun, S.-S. (1995). The composition of the Earth. *Chemical Geology* **120**, 223–253.

Meisel, T., Walker, R. J., Irving, A. J. & Lorand, J.-P. (2001). Osmium isotopic composition of mantle xenoliths: a global perspective. *Geochimica et Cosmochimica Acta* **65**, 1311–1323.

Menzies, A. H., Carlson, R. W., Shirey, S. B. & Gurney, J. J. (1999). Re–Os systematics of Newlands peridotite xenoliths: implications for diamond and lithosphere formation. In: Gurney, J. J., Gurney, J. L., Pascoe, M. D. & Richardson, S. H. (eds) *Proceedings of the 7th International Kimberlite Conference, Volume 2*. Cape Town: Red Roof, pp. 566–573.

Menzies, M., Rogers, N., Tindle, A. & Hawkesworth, C. J. (1987). Metasomatic and enrichment processes in lithospheric peridotites, an effect of asthenosphere–lithosphere interaction. In: Menzies, M. & Hawkesworth, C. J. (eds) *Mantle Metasomatism*. London: Academic Press, pp. 313–361.

Mitchell, R. H. (1973). Magnesian ilmenite and its role in kimberlite petrogenesis. *Journal of Geology* **81**, 301–311.

Moine, B. N., Grégoire, M., O'Reilly, S. Y., Sheppard, S. M. F. & Cottin, J.-Y. (2001). High field strength element fractionation in the upper mantle: evidence from amphibole-rich composite mantle xenoliths from the Kerguelen Islands (Indian Ocean). *Journal of Petrology* **42**, 2145–2167.

Moore, A. & Belousova, E. (2005). Crystallization of Cr-poor and Cr-rich megacryst suites from the host kimberlite magma: implications for mantle structure and the generation of kimberlite magmas. *Contributions to Mineralogy and Petrology* **149**, 462–481.

Neumann, E.-R., Wulff-Pedersen, E., Johnsen, K., Andersen, T. & Krogh, E. (1995). Petrogenesis of spinel harzburgite and dunite suite xenoliths from Lanzarote, eastern Canary Islands: implications for the upper mantle. *Lithos* **35**, 83–107.

Neumann, E.-R., Wulff-Pedersen, E., Pearson, N. J. & Spencer, E. A. (2002). Mantle xenoliths from Tenerife (Canary Islands): evidence for reactions between mantle peridotite and silicic carbonatite melts inducing Ca metasomatism. *Journal of Petrology* **43**, 825–857.

Nixon, P. H. & Boyd, F. R. (1973). Petrogenesis of the granular and sheared ultrabasic nodule suite in kimberlites. In: Nixon, P. H. (ed.) *Lesotho Kimberlites*. Maseru: Lesotho National Development Corporation, pp. 48–56.

Nowell, G. M., Pearson, D. G., Bell, D. R., Carlson, R. W., Smith, C. B., Kempton, P. D. & Noble, S. R. (2004). Hf isotope systematics of kimberlites and their megacrysts: new constraints on their source regions. *Journal of Petrology* **45**, 1583–1612.

Ohtani, E., Kawabe, I., Moriyama, J. & Nagata, Y. (1989). Partitioning of elements between majorite garnet and melt and implications for petrogenesis of komatiite. *Contributions to Mineralogy and Petrology* **103**, 263–269.

Pearce, N. J. G., Perkins, W. T., Westgate, J. A., Gorton, M. P., Jackson, S. E., Neal, C. R. & Chenery, S. P. (1997). A compilation of new and published major and trace element data for NIST SRM 610 and NIST SRM 612 glass reference materials. *Geostandards Newsletter* **21**, 115–144.

Pearson, D. G., Rogers, N. W., Irving, A. J., Smith, C. B. & Hawkesworth, C. J. (1995*a*). Source region of kimberlites and lamproites: constraints from Re–Os isotopes. Extended Abstracts of the 6th International Kimberlite Conference. Novosibirsk: Russian Academy of Sciences, United Institute of Geology, Geophysics and Mineralogy, pp. 430–432.

Pearson, D. G., Carlson, R. W., Shirey, S. B., Boyd, F. R. & Nixon, P. H. (1995*b*). Stabilisation of Archaean lithospheric mantle: a Re–Os isotope study of peridotite xenoliths from the Kaapvaal Craton. *Earth and Planetary Science Letters* **134**, 341–357.

Pearson, D. G., Canil, D. & Shirey, S. B. (2003). Mantle samples included in volcanic rocks: xenoliths and diamonds. In: Carlson, R. W. (ed.) *Treatise on Geochemistry: the Mantle and Core, Volume 2*. Amsterdam: Elsevier, pp. 171–275.

Rehfeldt, T., Obst, K. & Johansson, L. (2006). Petrogenesis of ultramafic and mafic xenoliths from Mesozoic basanites in southern Sweden: constraints from mineral chemistry. *International Journal of Earth Sciences* doi:10.1007/s00531-006-0116-4.

Roeder, P. L. & Emslie, R. F. (1970). Olivine–liquid equilibrium. *Contributions to Mineralogy and Petrology* **29**, 275–289.

Rudnick, R. L., McDonough, W. F. & Chappel, B. W. (1993). Carbonatite metasomatism in the northern Tanzania mantle: petrographic and geochemical characteristics. *Earth and Planetary Science Letters* **114**, 463–475.

Schmickler, B., Jacob, D. E. & Foley, S. F. (2004). Eclogite xenoliths from the Kuruman kimberlites, South Africa: geochemical fingerprinting of deep subduction and cumulate processes. *Lithos* **75**, 173–207.

Schmitz, M. D., Bowring, S. A., de Wit, M. J. & Gartz, V. (2004). Subduction and terrane collision stabilize the western Kaapvaal craton tectosphere 2·9 billion years ago. *Earth and Planetary Science Letters* **222**, 363–376.

Schulze, D. J. (1987). Megacrysts from alkalic volcanic rocks. In: Nixon, P. H. (ed.) *Mantle Xenoliths*. Chichester: John Wiley, pp. 433–451.

Scott, B. H. (1981). Kimberlite and lamproite dykes from Holsteinsborg, West Greenland. *Meddelelser om Grønland Geoscience* 3–24.

Scott Smith, B. H. (1987). Greenland. In: Nixon, P. H. (ed.) *Mantle Xenoliths*. Chichester: John Wiley, pp. 23–32.

Shirey, S. B., Carlson, R. W., Richardson, S. H., Menzies, A., Gurney, J. J., Pearson, D. G., Harris, J. W. & Wiechert, U. (2001). Archean emplacement of eclogitic components into the lithospheric mantle during formation of the Kaapvaal craton. *Geophysical Research Letters* **28**, 2509–2512.

Simon, N. S. C. (2004). The formation and modification of cratonic lithospheric roots—a petrological and geochemical study of xenoliths from the Kaapvaal Craton. PhD thesis, Vrije Universiteit Amsterdam, 251 pp.

Simon, N. S. C., Pearson, D. G., Carlson, R. W. & Davies, G. R. (2002). Origin of garnet and clinopyroxene in Kaapvaal low-T peridotite xenoliths: implications from secondary ionisation mass spectrometry (SIMS) data. *Geochimica et Cosmochimica Acta* **66**, A717–A717.

Simon, N. S. C., Irvine, G. J., Davies, G. R., Pearson, D. G. & Carlson, R. W. (2003). The origin of garnet and clinopyroxene in 'depleted' Kaapvaal peridotites. *Lithos* **71**, 289–322.

Simon, N. S. C., Carlson, R. W., Pearson, D. G. & Davies, G. R. (2007). The origin and evolution of the Kaapvaal Craton lithospheric mantle. *Journal of Petrology* **48**, 000–000.

Smith, C. B. (1983). Pb, Sr and Nd isotopic evidence for sources of southern African Cretaceous kimberlites. *Nature* **304**, 51–54.

Stachel, T., Viljoen, K. S., Brey, G. P. & Harris, J. W. (1998). Metasomatic processes in lherzolitic and harzburgitic domains of diamondiferous lithospheric mantle: REE in garnets from xenoliths and inclusions in diamonds. *Earth and Planetary Science Letters* **159**, 1–12.

Suhr, G. (1999). Melt migration under oceanic ridges: inferences from reactive transport modelling of upper mantle hosted dunites. *Journal of Petrology* **40**, 575–599.

Suhr, G., Seck, H. A., Shimizu, N., Günther, D. & Jenner, G. A. (1998). Infiltration of refractory melts into the lowermost oceanic crust: evidence from dunite- and gabbro-hosted clinopyroxenes in the Bay of Islands Ophiolite. *Contributions to Mineralogy and Petrology* **131**, 136–154.

Takahashi, E. (1986). Melting of dry peridotite KLB-1 up to 14 GPa: implications on the origin of peridotitic upper mantle. *Journal of Geophysical Research* **91**, 9367–9382.

Taylor, L. A. (1993). Evolution of the subcontinental mantle beneath the Kaapvaal Craton: a review of evidence for crustal subduction for Bellsbank eclogites. *Geologija i Geofizika: Naucnyj Zurnal* **34**, 25–47.

Thompson, R. N., Gibson, S. A., Dickin, A. P. & Smith, P. M. (2001). Early Cretaceous basalt and picrite dykes of the Southern Etendeka Region; NW Namibia: windows into the role of the Tristan Mantle Plume in Paraná–Etendeka magmatism. *Journal of Petrology* **42**, 2049–2081.

Van Achterbergh, E. (2004). Geochemical fingerprints of mantle metasomatism. PhD thesis, Macquarie University, Sydney, 223 pp.

Walker, R. J., Carlson, R. W., Shirey, S. B. & Boyd, F. R. (1989). Os, Sr, Nd and Pb isotope systematics of southern African peridotite xenoliths: implications for the chemical evolution of subcontinental mantle. *Geochimica et Cosmochimica Acta* **53**, 1583–1595.

Winterburn, P. A., Harte, B. & Gurney, J. J. (1990). Peridotite xenoliths from the Jagersfontein kimberlite pipe: I. Primary and primary–metasomatic mineralogy. *Geochimica et Cosmochimica Acta* **54**, 329–341.

Wyatt, B. A., Baumgartner, M., Ancker, E. & Grutter, H. (2004). Compositional classification of 'kimberlitic' and 'non-kimberlitic' ilmenite. *Lithos* **77**, 819–840.

Zack, T. & Brumm, R. (1998). Ilmenite/liquid partition coefficients of 26 trace elements determined through ilmenite/clinopyroxene partitioning in garnet pyroxenite. Extended Abstracts of the 7th International Kimberlite Conference. Cape Town: University of Cape Town, pp. 986–988.

Zack, T., Kronz, A., Foley, S. F. & Rivers, T. (2002). Trace element abundances in rutiles from eclogites and associated garnet mica schists. *Chemical Geology* **184**, 97–122.